J. Fluid Mech. (1997), *vol.* 333, *pp.* 161–195

On the structures in the near-wake region of an elevated turbulent jet in a crossflow

By OLIVIER S. EIFF† AND JAMES F. KEFFER

Department of Mechanical and Industrial Engineering, University of Toronto, Toronto, Ontario, Canada M5S 3G8

(Received 28 July 1995 and in revised form 4 October 1996)

A pattern-recognition technique, applied to multi-point simultaneous velocity measurements obtained with 45° X-wire anemometer probes, is used to extract and characterize the underlying organized motions, i.e. coherent structures, within the near-wake region of a turbulent round jet discharged perpendicularly from a pipe into a crossflow. This flow has been found to be quite complex owing to its three-dimensional nature and the interactions between several flow regions. Analyses of the underlying coherent structures, which play an important role in the physics of the flow, are still rare and are mostly based on flow-visualization techniques. Using a pattern-recognition technique in conjunction with hot-wire measurements, we recently examined the wake regions of the pipe and jet at levels near the tip of the pipe, and found that Kármán-like vortex structures in the wake of the pipe are locked to similar structures in the jet-wake. In this paper we expand upon our previous work and characterize these structures throughout the wake of the jet up into the region of the bent-over jet – a region where they have not been identified previously. The complex geometry of these structures in the wake of the jet as well as their interaction with the bent-over jet are discussed. The results show that these structures split before they link to similar structures on the opposite side of the symmetry plane in the jet region. The results further suggest that the vorticity due to the structures in the wake of the jet contributes to the motion of the well-known counter-rotating vortex pair.

1. Introduction

The jet in a crossflow is a flow with a wide range of applications owing to its ability to mix two streams of fluid efficiently. It is characterized by a strong three-dimensional flow field, complex interactions between two streams of fluids (i.e. jet fluid and crossflow fluid) and several interacting flow regions (i.e. the crossflow, the jet, the wake behind the jet, the pipe/orifice flow and the wall boundary layer). In the case of the jet in a crossflow discharged from an elevated source (e.g. a pipe or stack), the wake behind the stack presents an additional important flow region.

The mean statistical properties of jets emitted into crossflows from both ground-level sources and elevated sources have been examined in detail in the literature both from an experimental and numerical point of view, but with more attention focused on the ground-level case (e.g. Keffer & Baines 1963; Kamatoni & Greber 1972; Fearn & Weston 1974; Andreopoulos & Rodi 1984; Sykes, Lewellen & Parker 1986; Ni, Kawall & Ketter 1993). Examinations of the time-dependent coherent structures, however,

† Present address: Department of Mechanical Engineering, University of Waterloo, Waterloo, Ontario, Canada N2L 3G1.

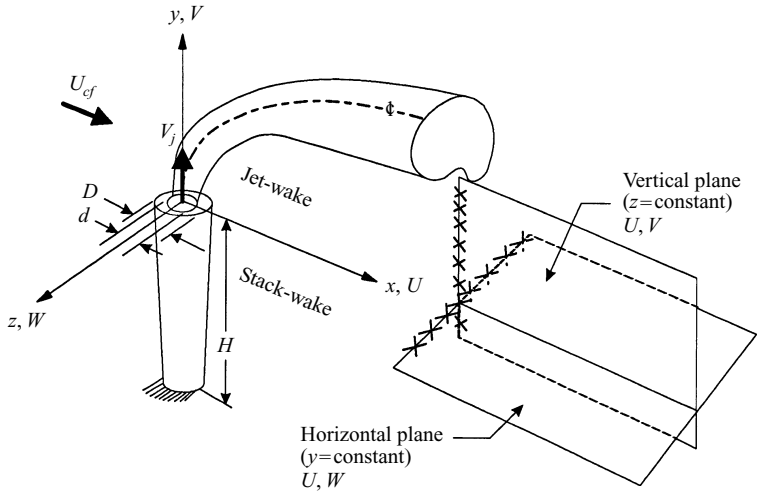

FIGURE 1. Definition sketch.

which underlie the physical processes responsible for mixing and entrainment, are still rare. The results available at present are limited to spectral measurements (e.g. McMahon, Hester & Palfrey 1971; Moussa, Trischka & Eskinazi 1977; Crabb, Durão & Whitelaw 1981) and, more recently, to flow-visualizations (Fric & Roshko 1994; Smith *et al.* 1993; Lozano *et al.* 1994; Huang & Chang 1994). Even more recent flow-visualization studies include those by Kelso, Lim & Perry (1996) and Morton & Ibbetson (1996). However, among all the studies only Moussa *et al.* (1977) and Huang & Chang (1994) considered the elevated case and none attempted a quantitative extraction of the coherent structures in either of the two flow cases. To the best of our knowledge, the first such study, focusing on the elevated case, was performed by Eiff, Kawall & Keffer (1995). Using measurements of velocities in conjunction with a pattern-recognition technique, we examined the interaction between the wake behind the stack and the wake behind the jet.

The emitted jet bends over into the crossflow direction, as shown in figure 1. On the downstream or lee side of the jet, a wake region is formed. In the case of a ground-level source, this wake region (the jet-wake) interacts with the ground-level boundary layer; interesting details of this interaction have recently been given with the flow-visualization results of Fric & Roshko (1994). In the case of the elevated source, the jet-wake interacts with the wake behind the stack (the stack-wake). The results of Eiff *et al.* (1995) examined this interaction at levels near the tip of a round cylindrical stack in detail. This included the stack-wake as well as the jet-wake.

One aspect of the flow which has received considerable attention (e.g. Fearn & Weston 1974; Kamatoni & Greber 1972) is the counter-rotating vortex pair. This is probably due to the fact that its mean motion can be measured directly without the need to ensemble-average any time-dependent motions. In this context, it can be described as a stationary structure. In the bent-over region of the jet, its primary plane of circulation is the (y, z) plane (x = constant). The fact, however, that the primary circulation appears stationary in the (x = constant)-planes hinders attempts to resolve the time-dependent motion in these planes. Nevertheless, we will try to shed more light on the nature of this structure, which is widely considered to be an important feature in the dynamics of this flow, by focusing on the two planes which are orthogonal to the x = constant plane.

The spectral results obtained by McMahon *et al.* (1971), Moussa *et al.* (1977) and Crabb *et al.* (1981) lead to the concept of 'vortex shedding' in the jet-wake, analogous to shedding behind solid bluff bodies. The results of Fric & Roshko (1994), Lozano *et al.* (1994) and Eiff *et al.* (1995) have shown direct evidence of such vortices in both the ground-level and elevated cases, although it appears that this 'vortex shedding' phenomenon is fundamentally different from shedding behind a solid bluff body. In the case of a ground-level jet, Fric & Roshko (1994) have concluded that it is the boundary layer on the wall (the ground-level) which is the source of vorticity for the vortices in the wake of the jet, i.e. 'it (the jet) does not appear to "shed" any of its vorticity'. In the case of an elevated jet, the results of Eiff *et al.* (1995), based on temperature measurements, indicated that the source of vorticity is the boundary layer on the inside surface of the stack, as opposed to the outside surface of the stack. The implication is that the jet does shed some of its vorticity, contrary to Fric & Roshko's conclusion. Results which support the idea that the jet also sheds some of its vorticity in the case of a ground-level source is given by Smith *et al.* (1993) and Lozano *et al.* (1994). Eiff *et al.* (1995) have shown continuous vortices extending from the stack-wake into the jet-wake. This phenomenon might at first be described as an extension of the stack-wake vortices into the jet-wake, which is what Fric & Roshko (1994) have suggested in their discussion of the results of Moussa *et al.* (1977). However, since according to Eiff *et al.* (1995) the origin of the vorticity of the jet-wake vortices is different to the origin of the vorticity of the stack-wake vortices, this phenomenon was described by the authors as a *lock-in* between two different sets of vortices.

The results of Eiff *et al.* (1995) clarified how the basically vertical vortices in the jet-wake (the jet-wake vortices) interact with the vortices in the stack-wake (the stack-wake vortices) below, but at this point there is no work known to us which suggests how these jet-wake vortices evolve in the region above the lower jet-wake region. Do they extend into the upper region of the jet-wake, into the region of the counter-rotating vortex pair or possibly into the core of the jet? The fact that they contain jet fluid implies that they must somehow be connected to the jet. These interactions are of fundamental importance as they are likely to influence the dispersion of jet fluid into cross-stream fluid. To address these issues, a cross-section of the near region of the flow, spanning the stack-wake, the jet-wake and the bend-over jet, is examined in detail with multi-point simultaneous X-wire velocity measurements in conjunction with a pattern-recognition technique.

2. Method of investigation

2.1. *Experimental details*

Measurements were performed in a variable-speed low-turbulence recirculating wind-tunnel at the Turbulent Research Group laboratory of the University of Toronto. This tunnel has a test section 3 m in length and 0.91 m × 1.52 m in cross-section with a speed range of about 1 m s^{-1} to 15 m s^{-1}. The jet was produced by means of a smooth pipe 0.43 m in length (H), 51 mm o.d. (D) and 32 mm i.d. (d) through which air at constant temperature was discharged at a velocity (V_j) of 18 m s^{-1}. The crossflow (wind tunnel) velocity, U_{cf}, was set so that R, the ratio of the crossflow velocity (U_{cf}) to the jet exit (V_j), was 3 (i.e. $U_{cf} = 6$ m s^{-1}). The turbulence intensity level of the crossflow was about 0.05%. The Reynolds number corresponding to the flow around the pipe was 20000, while the jet exit Reynolds number was 38000.

The pipe (i.e. the stack) was positioned at the upstream end and along the centreline of the tunnel and oriented perpendicularly to the crossflow. The Cartesian coordinate

	Type A	Type B	Type C
Plane	Horizontal	Vertical	Vertical
Rake position for y traverses	$x/D = 7$	$x/D = 7$, $z/D = -0.5$	$x/D = 7$, $z = 0$
Probe spacing	$\Delta z/D = 0.63$	$\Delta z/D = 0.63$	$\Delta z/D = 0.16$
Number of probes	8	8	6
Probe type	X-wire	X-wire	X-wire
Velocity components	U, W	U, V	U, V

TABLE 1. Summary of measurement configurations.

system employed here is centred at the tip and centre of the stack, with x in the streamwise (crossflow) direction, y in the lateral (vertical) direction and z in the spanwise direction (perpendicular to stack axis). See figure 1.

Multi-point simultaneous and instantaneous velocities were measured with rakes of Dantec 45° X-wires in several planes of the flow. Each signal was low-pass filtered at 2 kHz and digitized at a rate of 5000 points per second by means of a 12-bit A/D converter. The duration (T) of each signal processed was approximately 40 s or 200 000 points. The streamwise velocity (U) and lateral velocity (V) signals were obtained in vertical planes and U and spanwise velocity (W) signals were obtained in horizontal planes (see figure 1). The velocity measurements were performed at the streamwise station $x/D = 7$, where the jet is nearly bent-over (the inclination of the centreline of the jet is about 10° with respect to the horizontal at this location) such that accurate estimates of the velocities could be obtained with the X-wire probes aligned in the x-direction. The measurement configurations are summarized in table 1. For the vertical plane measurements, sets of measurements were taken with the rakes positioned at several z/D and y/D locations. The horizontal plane measurements were taken with the probes at fixed z/D locations and several y/D locations. The probe spacing in the rakes was either $0.16D$ or $0.63D$ as noted in table 1.

2.2. *General description of pattern-recognition technique*

The pattern-recognition technique (PRT) used in the present work is a modified version of the technique introduced by Mumford (1982) and Ferré & Giralt (1989) for detecting periodic or non-periodic coherent structures convecting past a set of probes. Application of the technique to a set of multi-point simultaneous flow-generated signals enables those portions of the signals that are due to the passage of the coherent structures to be identified and ensemble-averaged.

The detection of the coherent structures is based on the correlation between an initially prescribed velocity-vector pattern (template) and the set of measured signals. From a statistical analysis of the correlation, parts of the measured signals that are similar to the template are identified. These parts or realizations, which contain the instantaneous footprints of the structures, are then ensemble-averaged. The ensemble-averaged results are used as an improved template and correlated again with the original data signals. This process is continued in an iterative fashion until the velocities have converged. At this point, the most dominant structural features of the flow have been extracted. The result is normally independent of the original template, which essentially acts as a trigger.

2.3. *Signal decomposition*

The results presented in this work are based upon a triple decomposition of the flow. (This decomposition is referred to as the 'triple decomposition of the second kind' in Eiff *et al*. (1995) and as the 'double decomposition' by Hussain (1983).) For a velocity signal $P_i(t)$, this decomposition is based upon

$$P_i(t) = P_{cv} + p_{ci}(t) + P_{ri}(t),$$

where the subscript i refers to the ith probe in the rake, $P_i(t)$ refers to $U_i(t)$, $V_i(t)$ or $W_i(t)$, P_{cv} is the convection velocity of a coherent structure, $p_{ci}(t)$ is the coherent fluctuating velocity component, $p_{ri}(t)$ is the random or incoherent fluctuating velocity component. Ensemble-averaging the total fluctuating velocity components yields the ensemble-averaged coherent velocity components $\langle p_{ci} \rangle (s)$ and the random velocity components $p_{ri}(s)$. This decomposition yields the clearer quasi-Lagrangian view, owing to the fact that it enables the structures to be viewed in a frame of reference moving with their convection velocity. The streamwise convection velocities, U_{cv}, have been determined by using the PRT in a trial and error fashion with different convection velocities subtracted from the streamwise velocities until a peak is found in the number of realizations that are involved in the computation of the ensemble-average. In the horizontal planes the spanwise convection velocities are assumed to be negligible and in the vertical planes, as the flow has high mean lateral velocities, the lateral convection velocities have been approximated by the local $\bar{V}$.

2.4. *Ensemble-averaged vorticity*

The ensemble-averaged vorticity (i.e. the coherent vorticity)

$$\langle \omega_y \rangle = \frac{\partial \langle u_c \rangle}{\partial z} - \frac{\partial \langle w_c \rangle}{\partial x} \quad \text{or} \quad \langle \omega_z \rangle = \frac{\partial \langle u_c \rangle}{\partial y} - \frac{\partial \langle v_c \rangle}{\partial x},$$

where $\partial/\partial x = (1/U_{cv})/(\partial/\partial t)$ by Taylor's hypothesis, is estimated by taking central differences on the ensemble-averaged velocity vectors.

2.5. *Sectional streamlines*

In order to clarify some of the topological features in the vector plots, such as focal points which can be used to identify the presence of vortices (see Perry & Chong 1987), sectional streamlines have been computed and superimposed upon the vectors for a few selected vector plots. The streamlines are integrated from interpolated values of the ensemble-averaged velocity components shown in the vector plots, starting from selected points, (x_0, y_0) or (x_0, z_0). For instance, in the horizontal plane (x, z) the integration of the streamline equation,

$$\frac{\mathrm{d}x}{\langle u_c \rangle} = \frac{\mathrm{d}z}{\langle w_c \rangle},$$

is performed as

$$x(\zeta_1) = x_0 + \int_0^{\zeta_1} \langle u_c \rangle [x(\zeta), z(\zeta)] \, \mathrm{d}\zeta,$$

$$z(\zeta_1) = z_0 + \int_0^{\zeta_1} \langle w_c \rangle [x(\zeta), z(\zeta)] \, \mathrm{d}\zeta,$$

where ζ is a dummy variable. Theoretically, unless a streamline exits the window frame, it approaches a critical point in the limit. In the numerical integration, streamlines are

terminated when they reach the boundary of the computational domain indicated by the extent of the plots or when ζ_1 reaches an upper limit which restricts the length of the streamlines (for clarity of presentation).

2.6. *Fine-scale turbulence activity indicator function*

In order to distinguish free-stream ('potential') fluid from turbulent fluid a fine-scale turbulence activity indicator function (FSTIF) has been used. This function, introduced by Ferré *et al.* (1990) is very sensitive to fine-scale turbulent motion, while being basically insensitive to large-scale motions. It is based on the envelope of the second time derivatives of the instantaneous velocity signals and can be ensemble-averaged. FSTIF values have been offset and normalized by constants such that a FSTIF value of zero corresponds to the background turbulence of the wind tunnel.

2.7. *Presentation of pattern-recognition results*

On the plots showing the results of the pattern-recognition, time increases to the left, with the flow being from left to right. The spanwise and lateral positions of the probes in the horizontal and vertical planes respectively are normalized by D. An average convection velocity (U_0), where $U_0/U_{cf} = 0.92$, is used to convert the time coordinate into a spatial one. (As discussed in §2.3, the ensemble-averaged velocity vectors displayed in the plots are based on the set of measured signals from which the physical convection velocity, U_{cv}, has been subtracted. Since the use of U_0 only affects the scale of s, it is kept constant such that the streamwise separations of the structures at different planes in the flow can be compared directly, even when the physical convection velocity (U_{cv}) has varied. The value of 0.92 corresponds to the average convection velocity in the stack-wake and in the jet-wake.) The resulting streamwise spatial coordinate, s, is then normalized by D, i.e. $s = tU_0/D$. Iso-contour levels are plotted for $\pm 75\,\%$, $\pm 50\,\%$, $\pm 25\,\%$ and $\pm 10\,\%$ of the absolute peak value associated with each individual plot unless otherwise stated. To facilitate the interpretation of the results, grey-levels are assigned to the various iso-contour levels on several pattern-recognition plots. All velocities are normalized by U_{cf} and vorticity by U_{cf}/D. In the case of the vector plots, the smallest drawn vector is 10 % of the absolute peak velocity component. The scales of the components can be determined from the maximum values of the components shown below each plot. Furthermore, for clarity only every sixth velocity vector is plotted in the streamwise direction.

2.8. *Correlation length*

The correlation length (s_c) is the length s over which the initial template, as well as the subsequent improved templates, are correlated with the set of measured velocity signals for the purpose of selecting realizations. (With respect to the PRT plots we refer to the non-dimensional 'length' variable s, which is converted from the time coordinate, t, as indicated on the plots ($s = tU_0/D$).) The correlation length also determines the non-overlap condition for consecutively selected realizations. Therefore, the maximum frequency at which realizations are selected (i.e. the cut-off frequency) is given by $U_0/(s_c D)$.

The application of the templates over the specified correlation length is centred at $s = 0$. The actual width of the realizations selected and consequently the width of the final ensemble-averages (i.e. the 'window' length in the s-direction of the plots) is usually larger than the correlation length.

It was found that s_c has an influence on some of the horizontal plane results in the wake of the jet. This influence will be discussed in §§8 and 9.3.

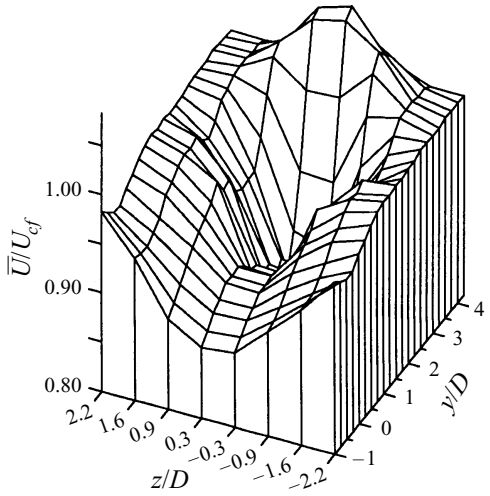

FIGURE 2. Three-dimensional representation $\bar{U}/U_{cf}(z)$ profiles at $x/D = 7$.

3. Mean velocity profiles

Before discussing the pattern-recognition results, it is helpful to examine the mean flow behaviour at the streamwise location that is being investigated in order to gain some familiarity with the extent and location of the different regions of the flow. Figure 2 shows a three-dimensional representation of $\bar{U}/U_{cf}(z)$ profiles obtained via the X-wire rake measurements (see table 1, type A for measurement configuration).

Figure 2 exhibits a maximum velocity excess at $y/D = 3.75$ and $z = 0$. Therefore this location coincides with the jet centreline of the nearly bent-over jet. For $y/D < 3.25$ a velocity deficit can be discerned, which is maximum at $y/D = 2.5$. Based on the velocity excess and deficit, the jet proper lies above $y/D = 3.25$ and the jet-wake between $y = 0$ and $y/D = 3.25$ (and the stack-wake below $y = 0$). As can be seen in figure 2, the mean wake deficit in the jet-wake and in the upper portion of the stack-wake is three-dimensional, with shear in both the y- and z-direction. It is therefore not unreasonable to expect the coherent structures which exist in this flow to be three-dimensional with strong components of vorticity in all three coordinate directions.

The location of the centre of the mean counter-rotating vortex pair was estimated to be near $y/D \sim 2.3$ with $\bar{W}$ measurements, in rough agreement ($y/D \sim 2$) with the results of Fearn & Weston (1974).

4. Horizontal plane results in the stack-wake

Previously, Eiff *et al.* (1995) investigated the interaction between the basically vertical vortices in the stack-wake and similar vortices in the jet-wake using spectral and pattern-recognition techniques. The PRT results spanned half the symmetric flow and consisted of ensemble-averaged velocities and turbulent fine-scale activity ($\langle$FSTIF$\rangle$) levels, but did not include vorticity or sectional streamlines. For the purposes of the present study, however, which focuses on the structures in the jet-wake, ensemble-averaged velocities in superposition with the associated ensemble-averaged vorticity iso-contours as well as sectional streamlines, provide a better means of studying the structures. In addition, in order to verify aspects of the vortex configuration proposed in §9.1, it was found that a horizontal rake which spans the width of the flow symmetrically is preferable to the asymmetrical one used in Eiff *et al.*

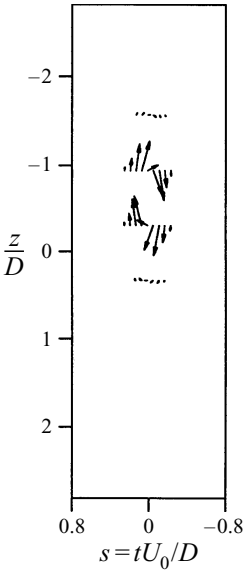

FIGURE 3. Clockwise-roller template.

(1995). Finally, it was discovered that the correlation length parameter (s_c) affects the results at certain locations in a significant way, while examining its effect also provides insight into the physics of the flow. Thus, a new set of measurements was taken with a wider rake of probes positioned symmetrically with respect to $z = 0$. These new measurements were taken for several lateral locations throughout the flow field (including the stack-wake, the jet-wake and the jet proper) and used to compute ensemble-averaged velocities, ensemble-averaged vorticity levels, ensemble-averaged turbulent fine-scale activity levels as well as sectional streamlines, all with several values of the correlation length.

In this section we present the first part of these new results obtained in the stack-wake with a short correlation length. The results will be compared in §8 with those obtained with a longer correlation length. Since the results are also part of a consistent set of results throughout the flow field, we will be able to make direct comparisons with the same type of results obtained in the jet-wake.

The measurements in the stack-wake were taken at $y/D = -1$, just below the tip of the stack. The details of the symmetric measurement configuration (type A) are given in table 1. The (short) correlation length used within the PRT is $s_c = 1.6$. The template used to obtain the first iteration is the clockwise-roller template shown in figure 3. The results of the sixth iteration have converged and are shown in figure 4. They consist of the ensemble-averaged velocity vector ($\langle u_c \rangle / U_{cf}\, \hat{\boldsymbol{i}} + \langle w_c \rangle / U_{cf}\, \hat{\boldsymbol{k}}$) pattern and sectional streamlines superimposed upon the ensemble-averaged vorticity iso-contours $\langle \omega_y \rangle / (U_{cf}/D)$.

The velocity-vector and sectional streamline patterns evident in figure 4 reveal several distinct regions of circulation, a clockwise circulation in the centre of the plot ($s = 0$) flanked by alternating clockwise and counter-clockwise circulations on each side. The negative vorticity iso-contours (lighter shades of grey) and the positive vorticity iso-contours (darker shades of grey), respectively, identify the clockwise and counter-clockwise motions which are present in the flow, in agreement with the senses of rotation implied by the ensemble-averaged velocity-vector pattern. From the

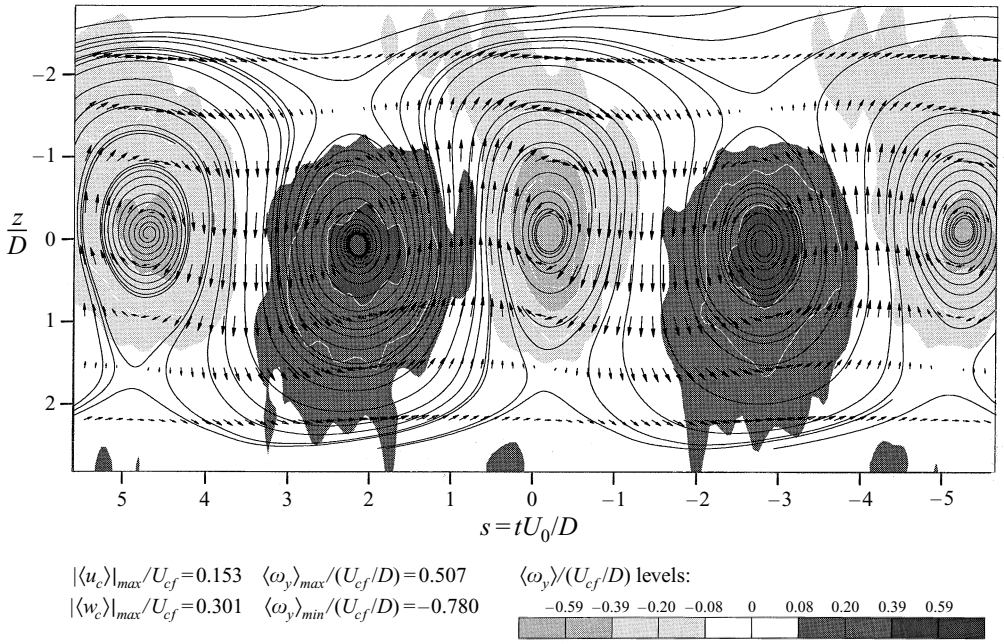

FIGURE 4. $\langle u_c\rangle/U_{cf}\,\hat{\boldsymbol{i}}+\langle w_c\rangle/U_{cf}\,\hat{\boldsymbol{k}}$ velocity vectors, sectional streamlines and $\langle\omega_y\rangle/(U_{cf}/D)$ vorticity iso-contours in horizontal plane at $x/D = 7$, $y/D = -1$. $s_c = 1.6$.

sectional streamline pattern the presence of foci (spirals) can be inferred, describing the presence of (coherent) vortices. Since the foci are congruent with the peak concentrations of coherent vorticity, it can be concluded that the correct convection velocity, U_{cv}, has been used. The observed streamline pattern and vorticity concentrations are the signatures of alternating and counter-rotating vortices expected in the near wake of a two-dimensional circular cylinder (e.g. Cantwell & Coles 1983; Zhou & Antonia 1993), and are often referred to as Kármán-like vortices. Thus, similar Kármán-like vortices are being shed near the tip of the stack in the same fashion as from a two-dimensional circular cylinder in spite of the three-dimensional wake deficit of the tip region, in agreement with the results of Eiff *et al.* (1995). This shedding is due to the presence of the emerging jet; equivalent PRT results behind a free-standing pipe with the same aspect ratio as the stack have shown that Kármán-like vortices do not exist at this location ($y/D = -1$).

Despite the structural similarities, we note that the lateral vortex spacing in the stack-wake is found to be about $0.1D$ (from the vorticity iso-contours in figure 4), which is less than the spacing in the wake behind a two-dimensional circular cylinder. (PRT results obtained from comparable measurements behind a circular cylinder at the same Reynolds number yielded a vortex spacing of about $0.3D$.)

5. Quasi-periodicity and its effect on the PRT results

The fact that adjacent structures other than the central structure have been extracted in figure 4 is an indication of the more or less constant phase between them, since the structures are 'periodically' occurring. The average shedding frequency, $f_s = U_0/sD$, deduced from the streamwise spacing s (≈ 4.85) between vorticity peaks of the same sign, yields a Strouhal number, $St_D = f_s D/U_{cf}$, of 0.19. This number is in good

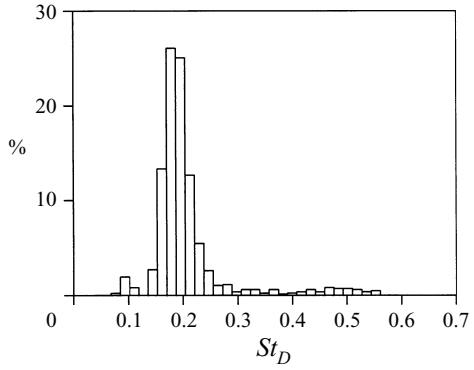

FIGURE 5. Percentage of detected realizations versus St_D based on detection frequencies in horizontal plane at $x/D = 7$, $y/D = -1$ with $s_c = 1.6$. Data correspond to results shown in figure 4.

agreement with the St_D numbers obtained from the peak frequencies of autospectra computed from the instantaneous fluctuating velocity components in the stack-wake and in the wake of a two-dimensional cylinder. As expected, the same St_D number was obtained by Eiff *et al.* (1995).

Instantaneous detection frequencies (f_{det}), which are the reciprocals of the periods between the selection of consecutive realizations, can provide more insight into the 'periodic' shedding process. These detection frequencies are converted into Strouhal numbers ($St_D = f_{det} D/U_{cf}$) and displayed in histograms. The histogram corresponding to the results shown in figure 4 is presented in figure 5. Since the total number of realizations or structures detected (N) exceeded 90% of the number of structures expected in the duration of the data set (T), i.e. $N/f_s T > 0.9$, this histogram is a good estimate of the actual Strouhal number probability density function (PDF). The histogram displays an almost bell-shaped distribution of the Strouhal numbers (i.e. of the shedding frequencies) centred around the mean Strouhal number (0.19) found by the autospectra and the spacing between the vorticity peaks. From the spread in Strouhal numbers it is evident that the physical process is not strictly periodic, but rather periodic with a random phase modulation. The shedding process is thus better described as quasi-periodic.

With the PRT, the extraction of the central structure (near $s = 0$) with respect to the plots does not depend on any periodicity of the structures, but the extraction of any adjacent structures within a repetitive structural pattern has to rely on such periodicity. With increasing random phase modulation (i.e. spread in the histograms) the ensemble-averages of the adjacent structures become increasingly compromised owing to smearing. The fact that the $\langle\omega_y\rangle/(U_{cf}/D)$ contours in figure 4 associated with the adjacent structures are similar to the $\langle\omega_y\rangle/(U_{cf}/D)$ contours associated with the central structure, is consistent with the relatively sharp distribution seen in the histograms in figure 5. It can be seen, however, that the peak $\langle\omega_y\rangle/(U_{cf}/D)$ levels of the adjacent structures are lower than those of the central ones. This apparent weakening is an indication of the quasi-periodicity.

6. Preliminary examination of horizontal planes in the jet-wake

A preliminary examination of the wake of the jet in a crossflow in several horizontal planes at increasing lateral (y/D) locations is made with a correlation length of $s_c = 1.6$. Type A measurements (refer to table 1) are used. The template used to extract

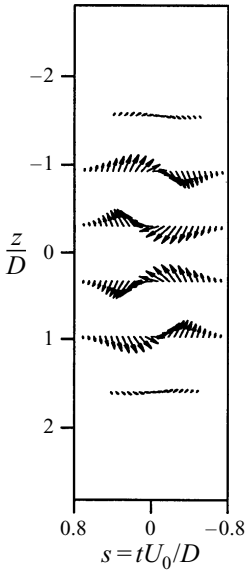

FIGURE 6. Double-roller template.

the patterns was the double-roller template shown in figure 6. It was chosen for its symmetry, so that the selection of structures would not be biased to one side of the symmetry plane. Essentially, however, the results were independent of the choice of template. Most of the observations made from the results in this section (§6) will be discussed in §§7, 8 and 9. Section 7 covers a preliminary examination of the vertical planes. Sections 8 and 9 include an analysis of the horizontal plane data with a correlation length of $s_c = 4.8$.

6.1. *Ensemble-averaged velocities and vorticity*

Figures 7(*a*) and 7(*b*), pertaining to the horizontal planes at $y/D = 1$ and $y/D = 3.25$, respectively, display the ensemble-averaged velocity vector ($\langle u_c \rangle / U_{cf}\, \hat{\boldsymbol{i}} + \langle w_c \rangle / U_{cf}\, \hat{\boldsymbol{k}}$) patterns and sectional streamlines superimposed upon the ensemble-averaged vorticity ($\langle \omega_y \rangle / (U_{cf}/D)$) iso-contours. The results in figure 7(*a*) show that a counter-clockwise vortex structure near $s = 0$ is clearly identified with a strong focus in the streamline pattern as well as the high concentration of vorticity. The strongly spiralling focus suggests that this structure is three-dimensional, i.e. it must be inclined with respect to the normal of the investigated plane (Perry & Chong 1987). This is consistent with our earlier results in Eiff *et al.* (1995) which concluded that the downstream inclination of the vortices in the jet-wake at this location was about 20°. According to those results we would also expect a clear alternating and counter-rotating Kármán-like vortex pattern at a Strouhal number based on the stack diameter (St_D) of 0.19, similar to the one observed behind the stack. In figure 7(*a*), however, the four adjacent patterns appear weak and badly smeared. Moreover, the streamwise spacings between the two clockwise structures and the central counter-clockwise one are higher than expected, suggesting a higher Strouhal number higher than 0.19. Nevertheless, in support of a Kármán-like vortex pattern, the vorticity iso-contours do indicate alternating and counter-rotating concentrations of vorticity. The reason behind the observed discrepancies in figure 7(*a*) to those expected by Eiff *et al.* (1995) will be discussed in §8.

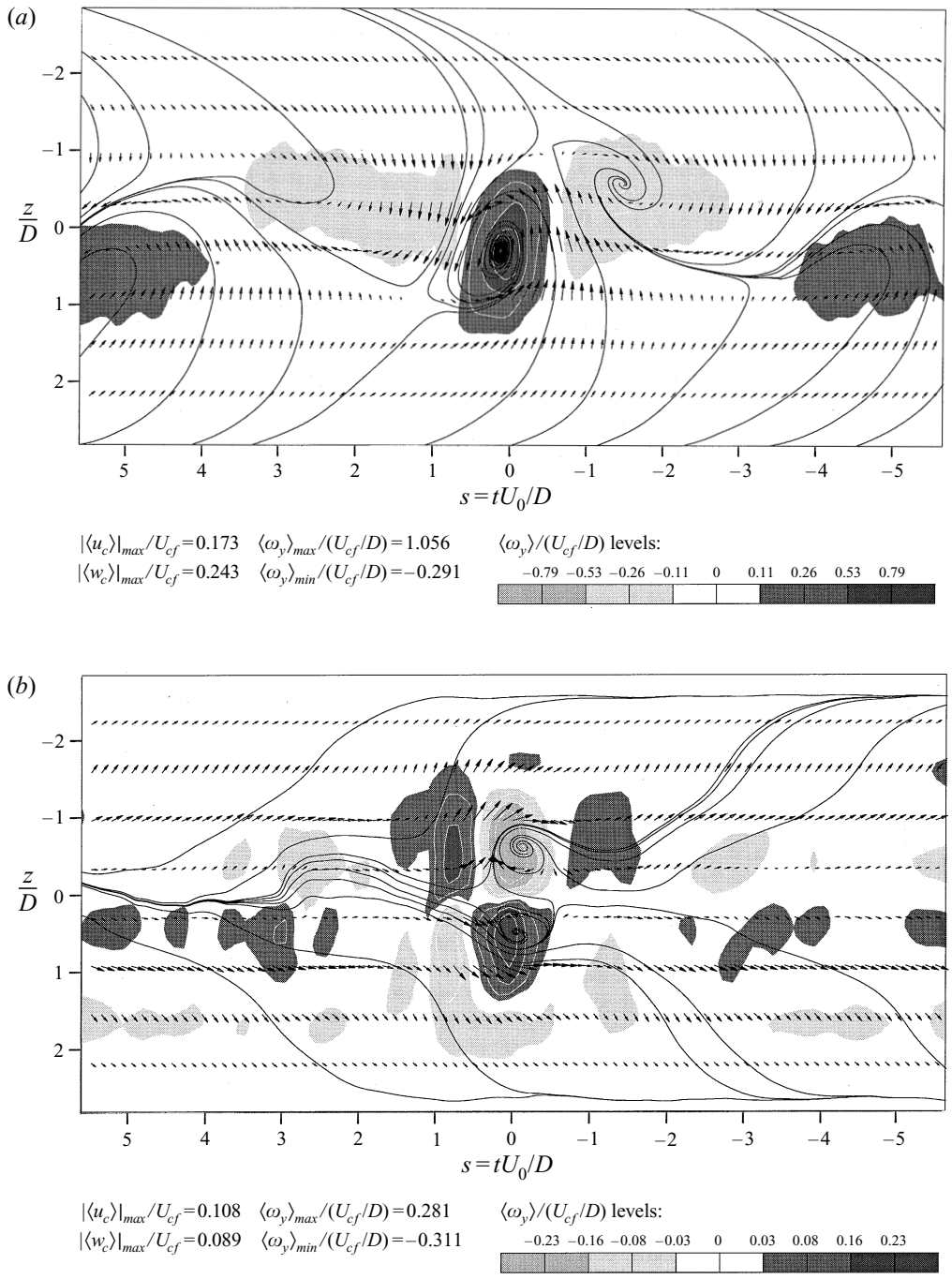

FIGURE 7. $\langle u_c\rangle/U_{cf}\,\hat{\boldsymbol{i}}+\langle w_c\rangle/U_{cf}\,\hat{\boldsymbol{k}}$ velocity vectors, sectional streamlines and $\langle\omega_y\rangle/(U_{cf}/D)$ vorticity iso-contours in two horizontal planes in the jet-wake at $x/D = 7$. (*a*) $y/D = 1$; (*b*) $y/D = 3.25$. $s_c = 1.6$.

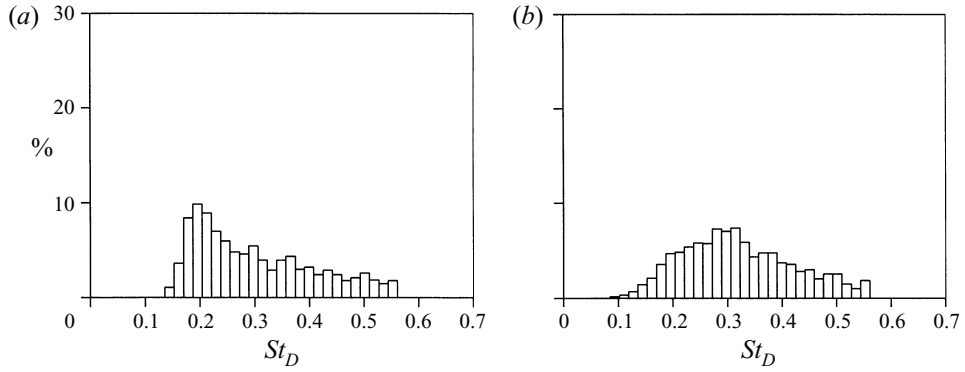

FIGURE 8. Percentage of detected realizations versus St_D based on detection frequencies in two horizontal planes at $x/D = 7$ with $s_c = 1.6$. (*a*) $y/D = 1$; (*b*) $y/D = 3.25$. Data correspond to results shown in figures 7(*a*) and 7(*b*), respectively.

Figure 7(*b*) shows the results obtained for the horizontal plane of the flow at $y/D = 3.25$. This location is at the upper limit of the jet-wake. Both clockwise and counter-clockwise vortices are evident near $s = 0$, resulting in a pattern which is more symmetric than alternating. Similarly, coherent vortices were also observed in all other horizontal planes lying between $y/D = 1$ and $y/D = 3.25$, but no vortices were observed in horizontal planes above $y/D = 3.25$. The results of Fric & Roshko (1994) and Lozano *et al.* (1994) have visualized the wake vortices only below the region of the mean counter-rotating vortex pair (centred near $y/D = 2.3$). If the vortices identified in the horizontal planes above $y/D \approx 2$ are indeed attributable to 'extensions' of the Kármán-like jet-wake vortices below, then these vortices extend to the upper limit of the jet-wake, penetrating the wake region of the jet which contains the mean counter-rotating vortex pair motion.

6.2. *Histograms*

Figures 8(*a*) and 8(*b*) show the histograms of the detection Strouhal numbers (St_D) based on the detection frequencies corresponding to figures 7(*a*) and 7(*b*). In figure 8(*a*), for $y/D = 1$, the peak Strouhal number is about 0.19, as expected. However, there is a significant skewness towards higher St_D numbers, which is likely to account for the smeared adjacent structures displayed in figure 7(*a*) as well as the reduced streamwise spacing between the structures resulting in a St_D number higher than 0.19. This will be shown in §8. In figure 8(*b*), at $y/D = 3.25$, the distribution of St_D numbers is also positively skewed and even the peak St_D number has shifted up towards 0.3. The corresponding ratios of the number of realizations or structures detected (N) to the total number of structures shed behind the stack, $N/f_s T$, is 1.35 at $y/D = 1$ and 1.5 at $y/D = 3.25$. Surprisingly, the ratios are higher than one. The reason for this, as well as the observed skewness in the histograms, will be discussed in §9.3.

6.3. *Peak vorticities*

The normalized peak vorticities, associated with the centres of the clockwise motions and the counter-clockwise motions, have been obtained from the maximum and minimum values of the ensemble-averaged vorticity contours of all horizontal planes analysed with $s_c = 1.6$ (e.g. figures 7(*a*) and 7(*b*)), and are plotted in figure 9. The $\langle\omega_y\rangle_{max}/(U_{cf}/D)$ peak vorticities are positive and correspond to the peak vorticities of the counter-clockwise structures. The $\langle\omega_y\rangle_{min}/(U_{cf}/D)$ peak vorticities are negative and correspond to the peak vorticities of the clockwise structures.

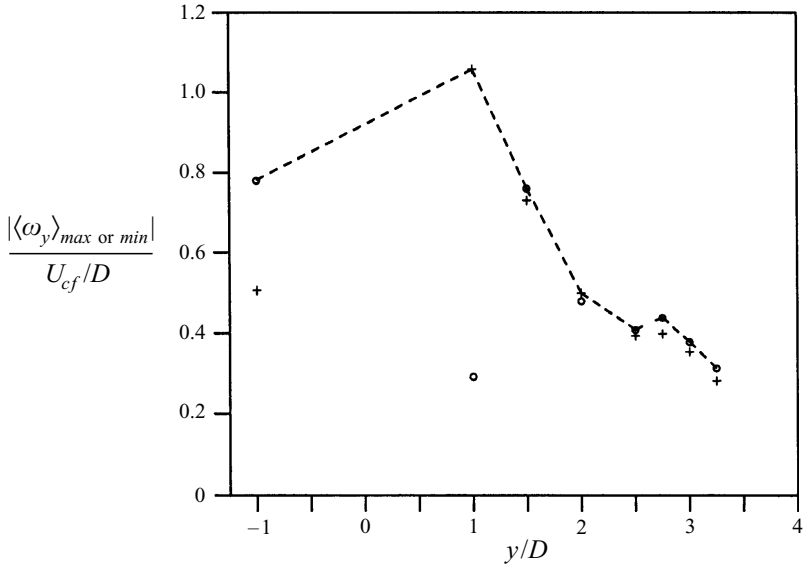

FIGURE 9. Absolute values of the peak vorticities associated with the horizontal plane results at $x/D = 7$ with $s_c = 1.6$ (e.g. figures 7(*a*) and 7(*b*)). +, $\langle\omega_y\rangle_{max}/(U_{cf}/D)$ is positive and corresponds to peak vorticities of counter-clockwise structures; ○, $\langle\omega_y\rangle_{min}/(U_{cf}/D)$, is negative and corresponds to peak vorticities of clockwise structures; ----, variation of absolute peak vorticities associated with structures centred near $s = 0$.

At $y/D = -1$ the absolute positive value is less than the absolute negative value since it is associated with the adjacent (counter-clockwise) structures. These appear weaker owing to the spread in shedding frequencies observed in the histogram (i.e. smearing in the ensemble-averaging process). (As expected, when the same data was analysed with a template of opposite circulation (counter-clockwise), the central structure extracted was counter-clockwise. Its absolute peak vorticity value was almost equal to the absolute peak vorticity value of the central clockwise structure obtained with the clockwise template (in figure 4).) At $y/D = 1$ the situation is reversed and more dramatic since the flow is even more quasi-periodic as the histogram shows, causing the adjacent (now clockwise) structures to be more smeared than at $y/D = -1$. For $y/D > 1$ planes, it was observed that both clockwise and counter-clockwise structures are centred around $s = 0$ within ± 1 (e.g. figure 7(*b*) at $y/D = 3.25$), yielding positive and negative peak vorticities of the same order.

Using the peak vorticities of the central structures near $s = 0$ (either clockwise or counter-clockwise) to avoid attenuation of the values owing to smearing, the dashed line in figure 9 can be drawn. Two features are noteworthy from the trends suggested by this curve. First, the peak vorticities decay with increasing y/D as the bent-over jet is approached. This decay could be caused by either an actual decay of vortex strength and/or an inclination of the vortex axis relative to the vertical. Secondly, the location of the largest peak vorticity is seen to be at $y/D = 1$. This suggests that the structures undergo vortex stretching near $y/D = 1$. Such vortex stretching would be consistent with the narrowing of the jet-wake deficit near $y/D = 1$ observed earlier in figure 2.

6.4. *Spanwise separation of centres of circulation*

From the focal points evident in figures 7(*a*) and 7(*b*) and similar horizontal plane results at all other y/D locations investigated, the average z/D locations of the centres of $\langle\omega_y\rangle$-circulation have been estimated. Figure 10 displays these average locations for

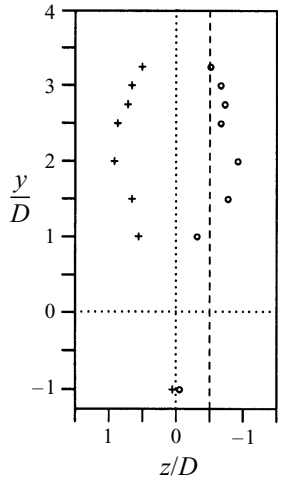

FIGURE 10. z/D locations of centres of $\langle\omega_y\rangle$-circulations deduced from horizontal plane results at $x/D = 7$ with $s_c = 1.6$ (e.g. figures 7(*a*) and 7(*b*)). +, counter-clockwise structures; ○, clockwise structures.

both the central clockwise and counter-clockwise vortical structures. It can be seen that the centres of $\langle\omega_y\rangle$-circulation are close to the symmetry plane ($z = 0$) near the tip of the stack and then diverge until around $y/D = 2.5$, above which they tend to approach the symmetry plane again.

7. Preliminary examination of vertical planes in jet-wake

The vertical plane PRT results in Eiff *et al.* (1995) allowed the Kármán-like vortex structures to be viewed from $y/D = -7.5$ to $y/D = 1.9$. It was shown that the vortex lines representing the structures are continuous from the boundary layer on the ground to at least $y/D = 1.9$, thus having given evidence of the kinematical aspect of the lock-in between the structures in the stack-wake and those in the jet-wake. These structures were observed to be quasi-two-dimensional in the (x, y) plane up to about $y/D = -1.2$. Above this point they bend downstream and appear to be inclined at about 20° to the vertical near the tip of the stack.

Although vortices with $\langle\omega_y\rangle$-circulation have been identified throughout the entire jet-wake region up to $y/D = 3.25$, it is not clear yet whether these vortices are in fact connected as might be expected.

Since Eiff *et al.* (1995) concluded that continuous vortex lines extend from the boundary layer on the ground into the jet-wake up to at least $y/D = 1.9$, it can be inferred that a line connecting the spanwise locations of the centres of $\langle\omega_y\rangle$-circulation regions depicted in figure 10 represents the z/D loci of such a vortex line up to at least $y/D \approx 2$. Assuming that a line connecting all locations of the centres of circulation in figure 10 represents a vortex line, one can draw a skeleton of the vortex that this vortex line would represent, as shown in figure 11. This is done simply to aid in visualizing the geometry and senses of rotation. It can be seen from the inferred (vortex) line in figure 10 that it crosses the $z/D = -0.5$ vertical plane (indicated by a dashed line in the (y, z)-plane) near $y/D = 1.2$ and near $y/D = 3.3$. With the aid of the vortex skeleton displayed in figure 11 it follows that in the $z/D = -0.5$ vertical plane a counter-clockwise circulation should be present near the lower 'intersection' point and a clockwise circulation near the upper 'intersection' point.

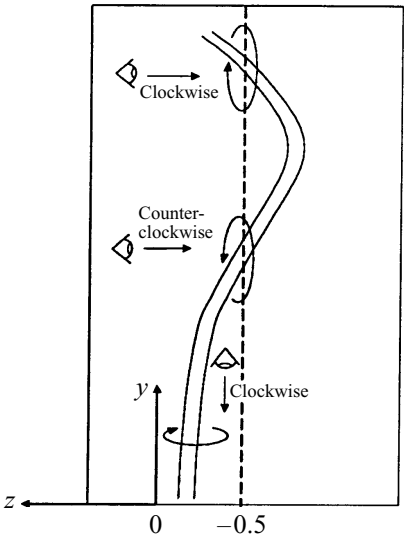

FIGURE 11. Vortex skeleton of a clockwise jet-wake vortex in the (y, z)-plane.

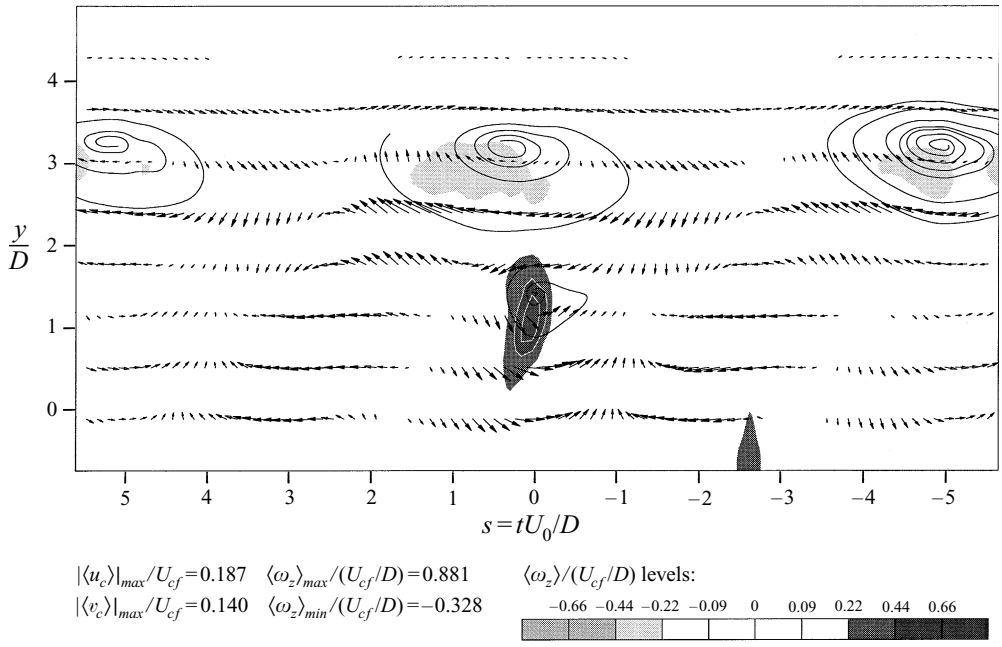

FIGURE 12. $\langle u_c\rangle/U_{cf}\,\hat{\boldsymbol{i}}+\langle v_c\rangle/U_{cf}\,\hat{\boldsymbol{j}}$ velocity vectors, sectional streamlines and $\langle\omega_z\rangle/(U_{cf}/D)$ vorticity iso-contours in vertical plane at $x/D = 7$, $z/D = -0.5$. $s_c = 1.6$.

Evidence of such circulations is given in the results presented in figure 12, which show the $\langle u_c\rangle/U_{cf}\,\hat{\boldsymbol{i}}+\langle v_c\rangle/U_{cf}\,\hat{\boldsymbol{j}}$ velocity vector pattern superimposed on the associated $\langle\omega_z\rangle/(U_{cf}/D)$ vorticity iso-contours, as well as sectional streamlines, in the $z/D = -0.5$ vertical plane. The results were based on type B measurements (table 1) and $s_c = 1.6$. A counter-clockwise roller template centred at the sixth probe from the top of the rake was used. It is evident from the streamline patterns that three clockwise

circulations occur around $y/D = 3$ and one counter-clockwise circulation around $y/D = 1.1$. These circulations confirm the existence and approximate locations of the circulations expected from the results presented in figure 10. Since both counter-clockwise and clockwise circulatory motions were educed, it follows that these motions occur in phase, on the average. The existence of this phase supports the idea that the two types of circulatory motion are connected and possibly due to one type of structure. Furthermore, since the presumption of the existence of a vortex line connecting the locations of the centres of circulation for $y/D > 2$ in figure 10 appears to be correct, it follows that the circulations observed for $y/D > 2$ in the horizontal plane results (e.g. figure 7(*b*) at $y/D = 3.25$) are indeed attributable to an 'extension' of the jet-wake vortices which were found up to $y/D \approx 2$. Thus, the jet-wake vortices are seen to penetrate a region of the flow which contains the mean counter-rotating vortex motion. This region is often regarded as the jet proper since it is visible if the jet fluid is seeded with a contaminant. According to the streamwise velocity deficit, however, it is still in the jet-wake region.

What is the streamwise inclination of the structures? From figure 12 three regions of clockwise circulation near $y/D = 3$ can be identified. It is thus possible that the structures extending from below are connected to either one of the top three. They could bend upstream, straight up, or downstream. This point will be discussed in §9.5.

8. Effect of correlation length

In order to demonstrate the basic effect of increasing the correlation length when the shedding distribution is quasi-periodic and skewed, the same data sets analysed previously at $y/D = -1$ (figure 4) and $y/D = 1$ (figure 7(*a*)) with $s_c = 1.6$ are re-examined using the same templates, but with $s_c = 4.8$. The resulting ensemble-averaged velocity vector ($\langle u_c \rangle / U_{cf}\, \hat{\boldsymbol{i}} + \langle w_c \rangle / U_{cf}\, \hat{\boldsymbol{k}}$) pattern and sectional streamlines superimposed upon the ensemble-averaged vorticity ($\langle \omega_y \rangle / (U_{cf}/D)$) iso-contours are shown in figures 13(*a*) and 13(*b*) for $y/D = -1$ and $y/D = 1$, respectively. The corresponding histograms of the detection Strouhal numbers are shown in figures 14(*a*) and 14(*b*).

In both histograms shown in figures 14(*a*) and 14(*b*) it can be seen that no realizations have been selected at $St_D > 0.19$. The detection of realizations at $St_D > 0.19$ in the histograms associated with the results obtained with $s_c = 1.6$ at the same lateral locations (recall the histograms shown in figure 5 and figure 8(*a*)) has effectively been eliminated by the use of $s_c = 4.8$. Instead, about half of the total number of realizations are selected at the first subharmonic ($St_D \sim 0.095$). Furthermore, the percentage of realizations selected is about half when the longer correlation length is used (with the long correlation length, $N/f_s T$ is about 0.5), but still exceeds the percentage of structures extracted by Hussain & Hayakawa (1987) in the wake of circular cylinder. Effectively, the elimination of detections at higher St_D is a consequence of the non-overlap condition in the correlation between the templates and the set of velocity signals. This condition is determined by the correlation length and was given in terms of the cut-frequency defined in §2.8. In terms of an St_D number, the cut-off is given by $U_0/U_{cf}\, s_c$, yielding 0.19 for $s_c = 4.8$.

A comparison of figure 4 (short correlation length) and figure 13(*a*) (long correlation length), both at $y/D = -1$, reveals essentially the same quasi-periodic vortex patterns at $St_D = 0.19$, although the peak vorticities in figure 13(*a*) associated with the central counter-clockwise and clockwise structures are now equal, as they should be physically. These peak vorticities are in agreement with the peak vorticity of the central clockwise structure in figure 4 (short correlation length), whereas, as mentioned earlier, the peak

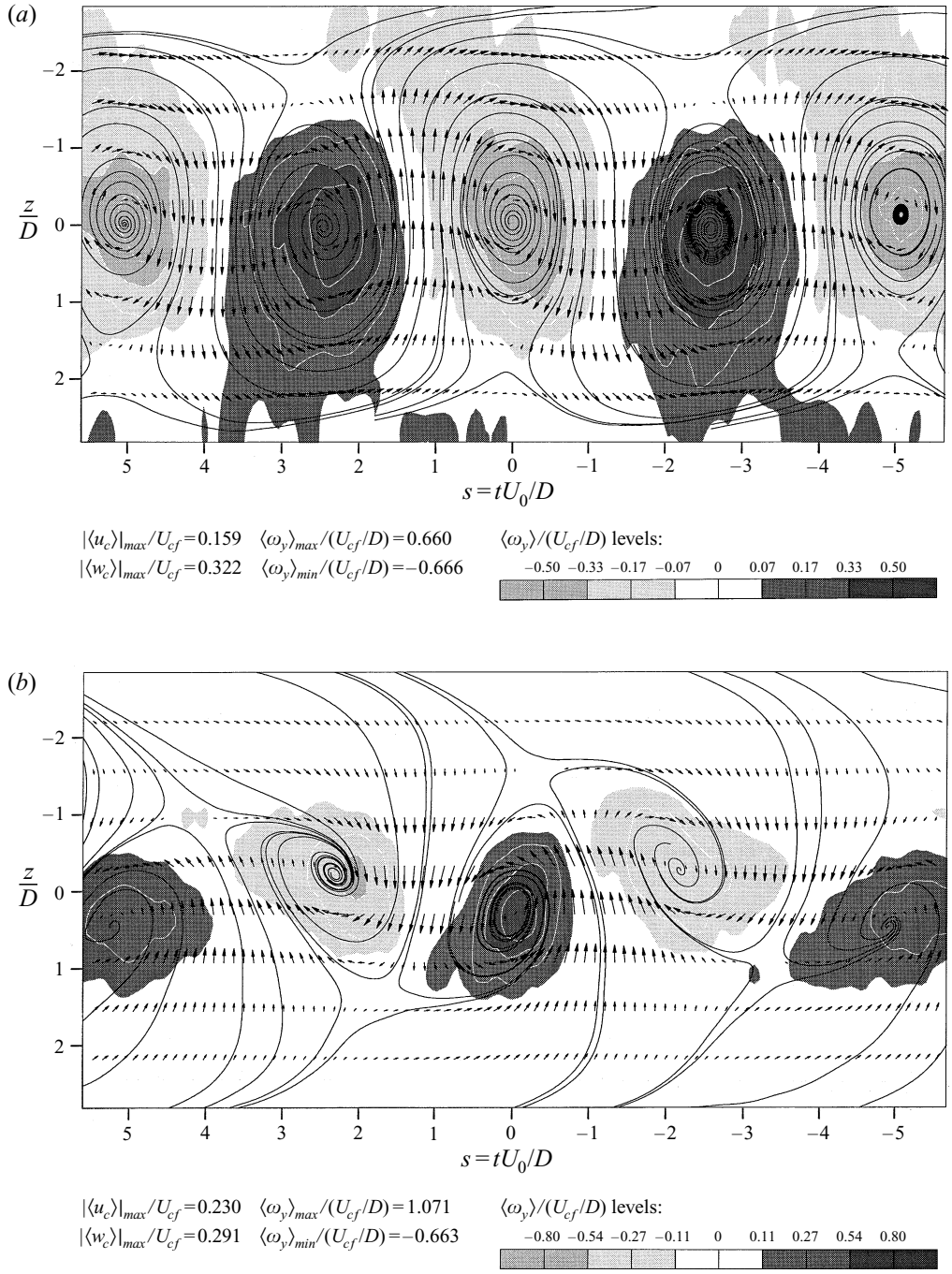

FIGURE 13. $\langle u_c\rangle/U_{cf}\,\hat{\boldsymbol{i}}+\langle w_c\rangle/U_{cf}\,\hat{\boldsymbol{k}}$ velocity vectors, sectional streamlines and $\langle\omega_y\rangle/(U_{cf}/D)$ vorticity iso-contours in two horizontal planes at $x/D = 7$. (*a*) $y/D = -1$; (*b*) $y/D = 1$. $s_c = 4.8$.

vorticities of the adjacent counter-clockwise structures in figure 4 are lower. Thus, by increasing the correlation length, the adjacent structures within the ensemble-averaged window have been extracted more clearly and their smearing has been minimized.

Comparing figure 7(*a*) (short correlation length) with figure 13(*b*) (long correlation

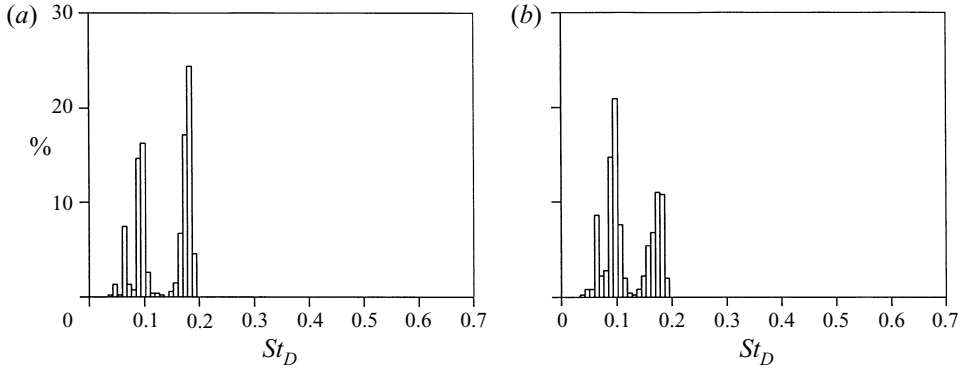

FIGURE 14. Percentage of detected realizations versus St_D based on detection frequencies in horizontal planes at $y/D = 7$ with $s_c = 4.8$. (*a*) $y/D = -1$; (*b*) $y/D = 1$. Data correspond to results shown in figures 13(*a*) and 13(*b*), respectively.

length), both at $y/D = 1$, one observes that the peak vorticities of the adjacent (clockwise) structures in figure 13(*b*) are closer to the value of the central (counter-clockwise) structure than in figure 7(*a*). Such an improvement was also observed at $y/D = -1$. More importantly, however, using the long correlation length at $y/D = 1$ results in a definite alternating and counter-rotating Kármán-like vortex pattern at $St_D = 0.19$, which was not clearly extracted with the short correlation length. This is not surprising when we consider the histogram obtained at $y/D = 1$ with the short correlation length (figure 8(*a*)). Its positively skewed detection Strouhal number distribution implies that there are a significant number of structures detected at the higher Strouhal numbers ($St_D > 0.19$) which are not added to the final ensemble-average when the long correlation length is used. With the short correlation length, these structures are included in the ensemble-average and cause smearing with a reduced streamwise separation between the ensemble-averaged structures in the PRT plots.

In summary, if the objective is to extract a quasi-periodic vortex pattern with a broad and positively skewed Strouhal number distribution, such that the smearing of 'adjacent' patterns is minimized, it is necessary to increase the correlation length appropriately. As it was our objective to extract the clearest possible adjacent patterns in order to confirm the frequency-doubling of the jet-wake vortex configuration discussed in the following section (§9), the remaining horizontal plane results will be based on the long correlation length ($s_c = 4.8$). The drawback of the 'low-pass filtering' effect (which results from the use of the long correlation length) is, of course, that structures passing the probes at instantaneously higher frequencies are being discarded. This issue will be addressed in §9.3.

It should be noted that tests with even longer correlation lengths have not revealed any significant changes in the ensemble-averaged results, except to further reduce the percentage of structures selected. Similarly, in the vertical planes, no significant improvement was obtained by increasing the correlation length to $s_c = 4.8$, and therefore the vertical plane measurements have been analysed with the short correlation length only ($s_c = 1.6$).

9. Linking and splitting of jet-wake vortex structures

In this section the detailed geometry of the jet-wake structures is discussed. In §9.1 the basic configuration of the structures is introduced. In §9.2, using the horizontal plane data with the long correlation length, evidence of the splitting of the jet-wake structures is given. In §9.3 the effect of the correlation length on the extraction of the vortex splitting is discussed. In §9.4 the linking of the jet-wake structures is examined. In §9.5 the inclination of the structures is resolved. Finally, in §9.6 the spanwise positions of the structures are discussed.

9.1. *Cross-link configuration*

On the basis of the solenoidal condition of the vorticity vector, vortex lines cannot terminate in a flow but must be interconnected or end on a solid or free surface. We can speculate, therefore, that the jet-wake structures from one side of the symmetry plane are in some fashion linked to ones from the other side. If so, they must cross the symmetry plane ($z = 0$) and form a 'bridge', similar to the top of a hairpin vortex. However, a central question arises: which structures are linked to form this bridge? Keeping in mind that all vortices have to be accounted for and that we expect symmetric conditions on both sides of the symmetry plane, a reasonable configuration is a cross-linked configuration, in which a typical Kármán-like jet-wake vortex structure on one side of the symmetry plane is linked to the preceding and the following jet-wake vortex structure on the opposite side. This, in turn, implies that at some lateral location the vortices have split. A typical and idealized vortex skeleton of the proposed cross-linked configuration is shown in figure 15.

9.2. *Vortex splitting*

For the reason given in §8, the following horizontal rake measurements of type A were examined with the long correlation length, $s_c = 4.8$. As before, the double-roller template displayed in figure 6 was used. The resulting ensemble-averaged velocity vector ($\langle u_c \rangle / U_{cf}\, \hat{\boldsymbol{i}} + \langle w_c \rangle / U_{cf}\, \hat{\boldsymbol{k}}$) pattern and sectional streamlines superimposed upon the ensemble-averaged vorticity ($\langle \omega_y \rangle / U_{cf}$) iso-contours at $y/D = 2$, 2.5 and 2.75 are shown in figures 16(*a*)–16(*c*), respectively.

Figure 16(*a*), at $y/D = 2$, shows vorticity iso-contours characteristic of alternating clockwise and counter-clockwise Kármán-like vortices. The sectional streamlines reveal a topology which resembles that of the stack-wave, more so than at $y/D = 1$. The shedding is still characterized by the Strouhal number, St_D, of 0.19.

At $y/D = 2.5$ (figure 16*b*) the regions of vorticity appear to be more distorted in the streamwise direction. Indeed, the central negative and positive vorticity lobes contain two regions of peak vorticity, suggesting that there might be two parallel vortices. This is confirmed by the sectional streamlines which show that, buried within the larger central clockwise circulation zone, there are two weak circulation zones of the same sign. Evidently, vortices close to the splitting point have been extracted. The centre of the vortex is already split, but the 'bulk' of the vortex fluid is still joined. The sectional streamlines of the central counter-clockwise vortices do not display evidence of splitting, but the shape of the streamlines shows that the structures are significantly stretched in the streamwise direction, suggesting that there exists an underlying splitting which is significantly smeared. This is supported by the positive vorticity iso-contours which do display two regions of peak vorticity. The sectional streamlines are apparently more sensitive to smearing than vorticity iso-contours.

Figure 16(*c*), at $y/D = 2.75$, shows that at least the clockwise Kármán-like vortices

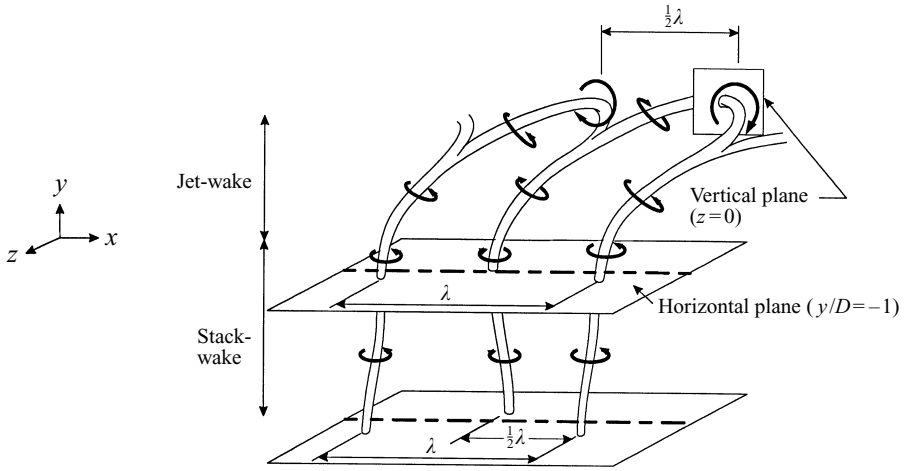

FIGURE 15. Vortex skeleton of the cross-linked jet-wake vortex configuration, including the stack-wake vortices.

have split. Three relatively strong clockwise circulation zones can be identified with corresponding concentrated regions of vorticity, which are spaced half a Strouhal period apart, i.e. $St_D \sim 0.38$. This is the average spacing we expect from the cross-link configuration after the vortices have split. Also, opposite Kármán-like vortices have aligned themselves symmetrically as can be seen by the central clockwise and counter-clockwise structures. This is not surprising as they should form a bridge less than one diameter above this lateral location.

The splitting of the adjacent counter-clockwise structures at $y/D = 2.75$, as observed at $y/D = 2.5$, is not as clearly defined by the PRT results as the splitting of the clockwise ones. These structures appear highly smeared. However, the streamwise extent of the adjacent vorticity iso-contours and the elongated shape of the streamlines suggest that the counter-clockwise vortices are also split. The splitting of the counter-clockwise vortices was verified by using the mirror image of the second to last iteration of the vectors shown in figure 16(*c*) as a template. A mirror image of the results displayed in figure 16(*c*) was obtained, verifying that the splitting occurs on both sides of the wake. Thus, the inability to show clearly the splitting of vortices other than the central one (near $s = 0$) is a result of smearing. The underlying reason for this smearing is that the phase differences between an 'original' Kármán-like vortex and the branched-off vortex are quite random. Such randomness is likely to be introduced directly by the degree of separation and by lateral variations in the branch point.

9.3. *Effect of correlation length on extraction of the vortex splitting*

A comparison of the horizontal plane results obtained with the short and long correlation lengths at $y/D = 1$, 2, 2.5, 2.75 and 3.25 reveals interesting details with regard to the vortex splitting.

As noted in §6.2, when the short correlation length is used at $y/D = 1$, the ratio of the number of structures selected to the number of structures shed behind the stack, $N/f_s T$, is 1.35 or 135%. This implies that at least 35% of the vortices have started to split, assuming that 100% of the original vortices have been selected. As a result, however, of selecting original as well as split vortices, the detection frequencies will necessarily be skewed towards frequencies higher than the nominal Strouhal frequency

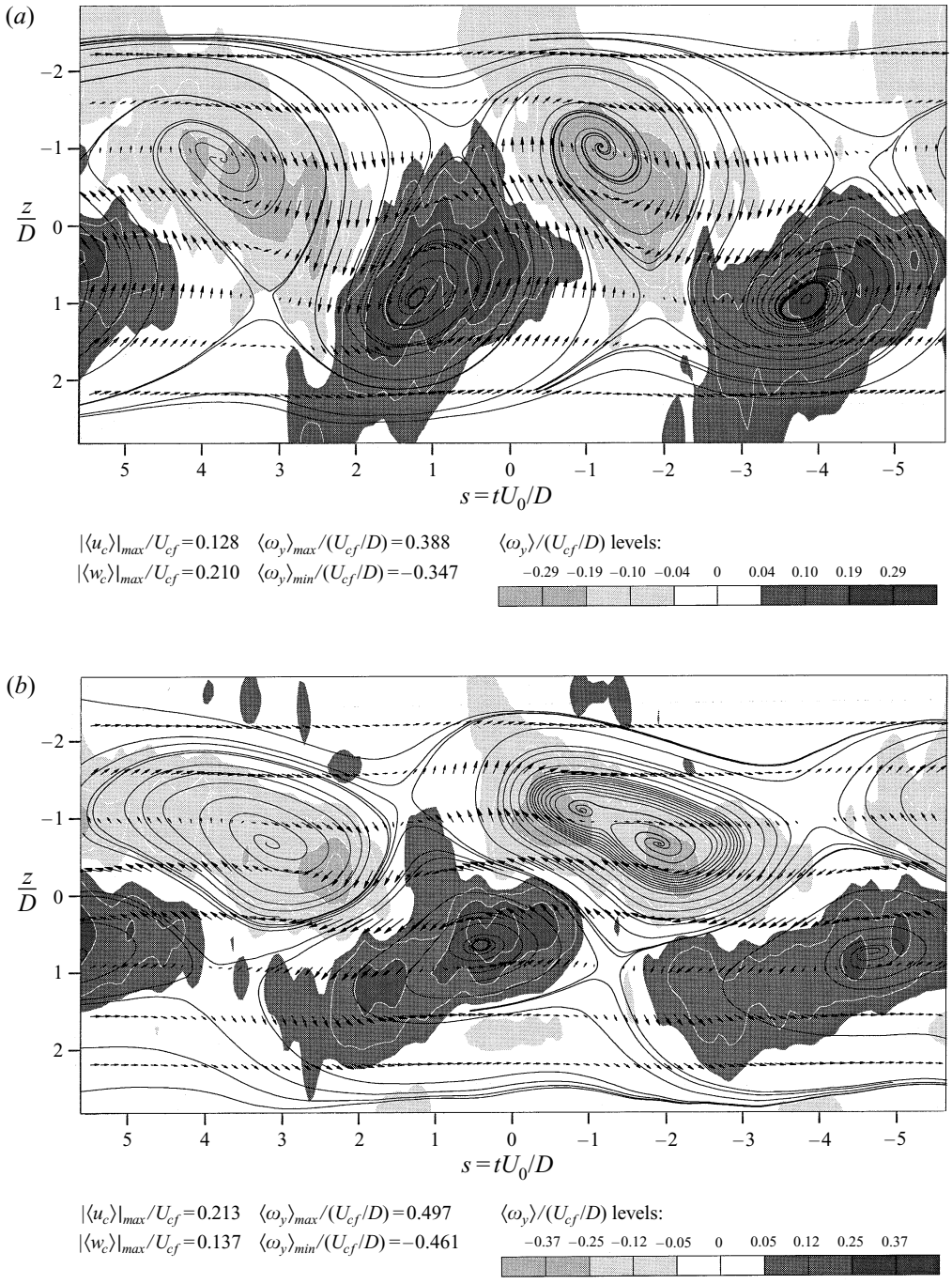

FIGURE 16(*a*, *b*). For caption see facing page.

(as seen in figure 8*a*). In fact, frequencies higher than twice the nominal Strouhal frequency (i.e. $St_D > 0.38$) are expected when the vortices have just split (and are therefore still close to each other). As a consequence of this splitting process only the selected vortices centred near $s = 0$ will be well aligned, but the adjacent structures will

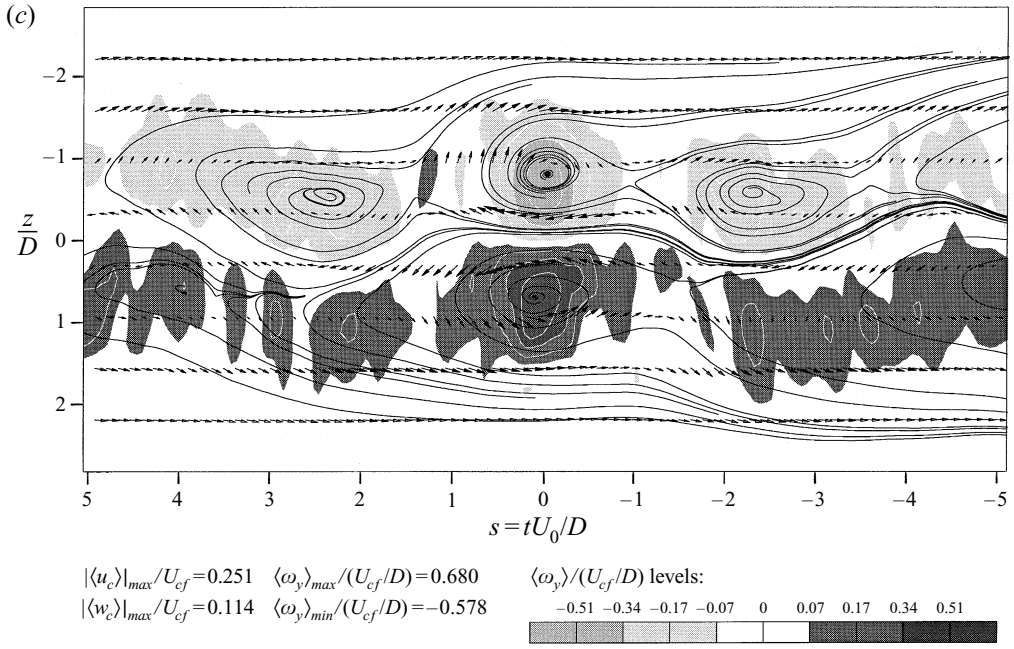

FIGURE 16. $\langle u_c\rangle/U_{cf}\,\hat{\boldsymbol{i}}+\langle w_c\rangle/U_{cf}\,\hat{\boldsymbol{k}}$ velocity vectors, sectional streamlines and $\langle\omega_y\rangle/(U_{cf}/D)$ vorticity iso-contours in three horizontal planes at $x/D = 7$. (*a*) $y/D = 2$; (*b*) $y/D = 2.5$; (*c*) $y/D = 2.75$. $s_c = 4.8$.

be highly smeared (as seen in figure 7*a*). Yet, the split vortices must also be relatively weak and occur randomly as there is no evidence of them in the results with the long correlation length (see figure 13*b*). In other words, the splitting process is just starting at this location.

Ensemble-averaged results at $y/D = 2$ obtained with the short correlation length (Eiff 1996) suggest a streamwise vortex spacing equivalent to $St_D > 0.19$, similar to figure 7(*a*) at $y/D = 1$, while with the long correlation length (see figure 16*a*) $St_D = 0.19$ is obtained. Evidently, the use of the longer correlation length allows a clearer extraction of the quasi-periodically occurring alternating vortex pattern at $y/D = 2$, in the same manner as discussed in §8 for $y/D = 1$. At $y/D = 2.5$, the use of the short correlation length resulted in patterns (Eiff 1996) that were similar to the ones obtained at $y/D = 2.75$ with the long correlation length (figure 16*c*), i.e. structures which are already well split. However, with the long correlation length at $y/D = 2.5$ (figure 16*b*), the extracted structures are just above the splitting point. By $y/D = 2.75$, the use of either correlation length yields essentially the same results, i.e. split vortices arranged in an almost aligned counter-rotating vortex pair pattern, although the use of the long correlation length reveals the underlying quasi-periodicity better. At $y/D = 3.25$, the results with either correlation length are too smeared to reveal evidence of the quasi-periodicity, but both results clearly show a well-aligned counter-rotating vortex pair pattern characteristic of the split vortices (e.g. figure 7*b*).

In summary, the largest influence of the correlation length is observed at $y/D = 1$. At this location the vortices are relatively strong owing to vortex stretching, and the use of the short correlation length reveals that as much as 35% of the vortices have started to split. The use of the long correlation length, however, avoids selecting the instances when the vortices split, and the final result up to $y/D = 2$ is the underlying

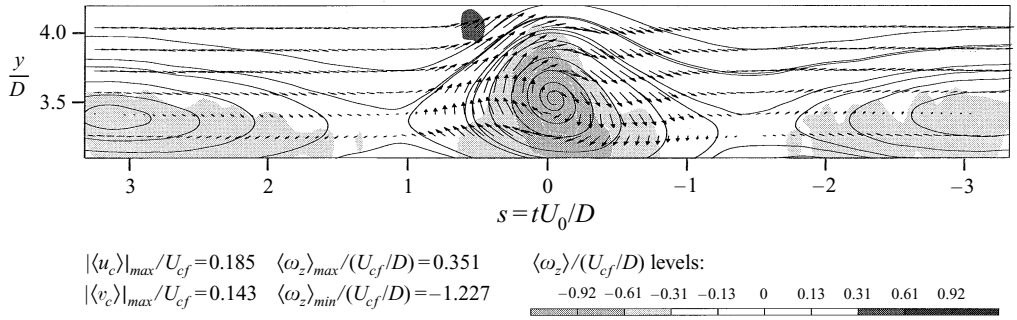

FIGURE 17. $\langle u_c\rangle/U_{cf}\,\hat{\boldsymbol{i}}+\langle v_c\rangle/U_{cf}\,\hat{\boldsymbol{j}}$ velocity vectors, sectional streamlines and $\langle\omega_z\rangle/(U_{cf}/D)$ vorticity iso-contours in vertical plane at $x/D = 7$, $z/D = 0$. $s_c = 1.6$.

quasi-periodic alternating vortex-pattern occurring at $St_D = 0.19$. Only at $y/D = 2.5$ are there enough well-aligned and/or strong split vortices such that the splitting is revealed directly with either correlation length. However, the differences between the results suggest that the process is still not completed (with the long correlation length, the extracted vortices are just above the splitting point, but with the short correlation length, they are already split). By $y/D = 2.75$ the process appears to be almost completed since either correlation length reveals essentially the same counter-rotating vortex pattern, except that the adjacent structures are not as smeared with the long correlation length. At $y/D = 3.25$, coinciding with the upper edge of the jet-wake, the process is completed since both reveal a symmetric counter-rotating vortex pair characteristic of split vortices and the overall influence of the correlation length on the resulting patterns is negligible. Yet, application of the short correlation length results in a higher $N/f_s\,T$ ratio, equal to 1.5 (the ratio with the long correlation length is about 0.5 throughout the jet-wake), implying that as many as 50% of the completely split vortices have been detected.

9.4. *Linking*

According to the cross-link configuration (see figure 15), rake measurements in the symmetry plane ($z = 0$), which are effectively a cut through the top of the bridges, are expected to reveal clockwise circulation regions. To pursue this aspect, a set of type C vertical rake measurements was taken in the symmetry plane (refer to table 1). The probe spacing for type C measurements was a quarter of that of the other types for better resolution of the structures. The correlation length, s_c, was 1.6. The results, comprising the $\langle u_c\rangle/U_{cf}\,\hat{\boldsymbol{i}}+\langle v_c\rangle/U_{cf}\,\hat{\boldsymbol{j}}$ pattern, $\langle\omega_z\rangle/(U_{cf}/D)$ and sectional streamlines, are presented in figure 17.

Clearly, a clockwise circulation pattern near $s = 0$ centred around $y/D = 3.5$ can be identified. This suggests that the bridging (or linking) aspect of the above speculation is correct, i.e. the vortex lines of the jet-wake vortices on either side of the symmetry plane extend up beyond $y/D = 3.25$ and cross the symmetry plane ($z = 0$) around $y/D = 3.5$, on the average. This cross-over point is just below the jet centreline ($y/D = 3.75$).

The frequency associated with the repeated clockwise circulation regions is about $St_D = 0.3$, somewhat below the nominal Strouhal number of the split vortices, $St_D = 0.38$. It can also be observed that the adjacent regions of circulations are slightly lower than the central one. This lower location suggests that owing to variations in the lateral and spanwise location of the bridges, a significant number of bridges occur

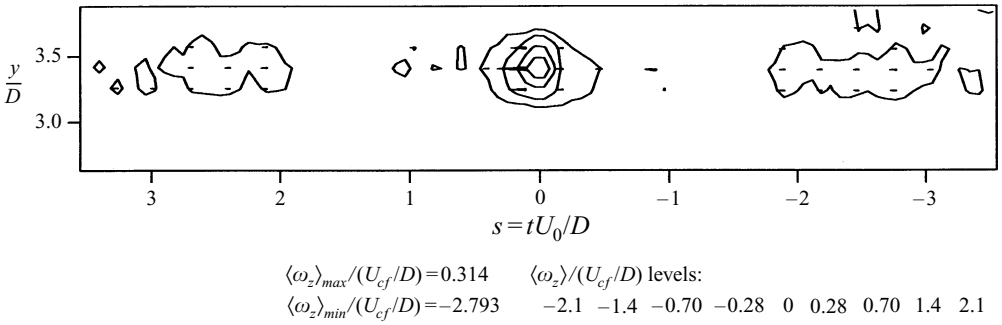

FIGURE 18. $\langle\omega_z\rangle/(U_{cf}/D)$ vorticity iso-contours in vertical plane at $x/D = 7$, $z/D = 0$. $s_c = 1.6$. The clockwise template used had nine probes, i.e. three 'fictional probes' for lateral alignment.

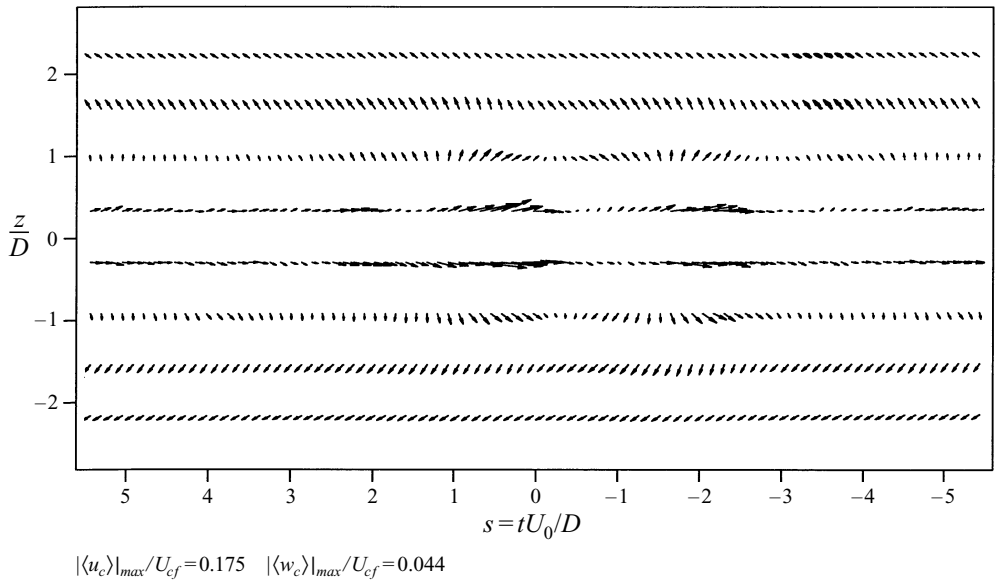

FIGURE 19. $\langle u_c\rangle/U_{cf}\,\hat{\boldsymbol{i}}+\langle w_c\rangle/U_{cf}\,\hat{\boldsymbol{k}}$ velocity vectors in horizontal plane at $x/D = 7$, $y/D = 3.75$. $s_c = 4.8$.

below $y/D = 3.5$. These variations can cause the streamwise period between adjacent structures to be highly smeared and to appear larger than the nominal period equivalent to $St_D = 0.38$ (i.e. $St_D < 0.38$).

To verify that these bridges do indeed occur at $St_D \sim 0.38$, the realizations were allowed to be aligned in the lateral direction by adding three fictional 'probes' to the clockwise template (see Ferré & Giralt 1989). The resulting $\langle\omega_z/(U_{cf}/D)\rangle$ vorticity iso-contours are shown in figure 18. The regions of concentrated vorticity which are associated with the clockwise circulatory motions are now spaced about $s = 2.4$ apart, equivalent to $St_D \sim 0.38$.

Considering that the structures cross the symmetry plane near $y/D = 3.5$, we do not expect any circulation in the horizontal planes above $y/D = 3.5$. Specifically, the predominant velocities associated with the clockwise motion of the bridges in a horizontal plane at $y/D = 3.75$ (the centreline of the nearly bent-over jet) should be positive streamwise velocities. Figure 19 shows the $\langle u_c\rangle/U_{cf}\,\hat{\boldsymbol{i}}+\langle w_c\rangle/U_{cf}\,\hat{\boldsymbol{k}}$ pattern at $y/D = 3.75$ obtained from type A measurements, using the double-roller template

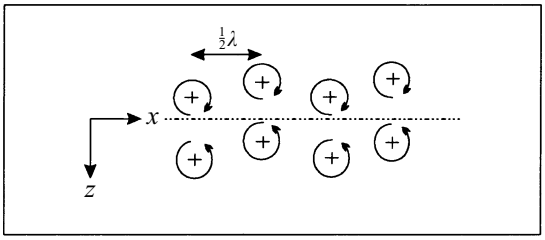

FIGURE 20. Schematic representation of asymmetrically alternating counter-rotating vortex pattern observed in figure 16(*c*) at $y/D = 2.75$.

(figure 6) and $s_c = 4.8$. Strong positive streamwise velocities are clearly identifiable near $s \sim 0$ and near $s \sim \pm 2.5$. The slight outward-pointing velocity vectors are also in agreement with the curvature of the bridges. The period between the streamwise velocity concentrations reconfirms the expected occurrence of the bridges at $St_D \sim 0.38$.

9.5. *Inclination of structures*

Figure 7(*b*), introduced in §6.1, showed the $\langle\omega_y\rangle/(U_{cf}/D)$ vorticity iso-contours, superimposed upon the $\langle u_c\rangle/U_{cf}\,\hat{\boldsymbol{i}} + \langle w_c\rangle/U_{cf}\,\hat{\boldsymbol{k}}$ velocity-vector pattern and sectional streamlines in the horizontal plane at $y/D = 3.25$. These results were obtained with $s_c = 1.6$. As discussed previously, most vortices are split at this point and either correlation length yields essentially the same results. In figure 7(*b*), only one central counter-rotating vortex pair can be identified; any adjacent structures are significantly smeared. It can also be observed, that, with respect to either the central clockwise or the counter-clockwise structures, the upstream outward $\langle w_c\rangle/U_{cf}$ velocities are higher than the downstream inward $\langle w_c\rangle/U_{cf}$ velocities. These features are characteristic of streamwise as well as inwardly inclined horseshoe-like structures as viewed in a horizontal plane view, which reveals a cross-section of the counter-rotating 'legs' of the horseshoe-like structures. Another characteristic feature of horseshoe-like structures is the strong backflow between the two counter-rotating legs. This feature is essentially due to the bridging aspect of horseshoe-like jet-wake vortices. Kopp, Kawall & Keffer (1995) modelled an inclined horseshoe-like vortex via a Λ-vortex model with straight legs, which essentially displayed the same features (refer to figure 3(*c*) in Kopp *et al.* 1995). Thus, there is evidence that the circulations identified here are the 'footprints' of horseshoe-like structures which are inclined positively into the streamwise direction, as suggested by the vortex skeleton of the cross-link configuration shown in figure 15. More evidence will be given in §10.

9.6. *Antisymmetry*

The spanwise (y/D) spacing of the jet-wake vortices has already been presented in §6.4 (figure 10). Although the spacing was found to be varying with lateral (y/D) location, the vortices were roughly symmetric with respect to the symmetry plane ($z = 0$). The vortex spacings in figure 10 were based on the centres of $\langle\omega_y\rangle$-circulation obtained with the PRT results in the horizontal planes using the short correlation length. Inspection of the PRT results obtained in the horizontal planes, but using the long correlation length (e.g. figure 16(*c*) at $y/D = 2.75$), reveals that the spanwise positions of the counter-rotating vortex pairs after the jet-wake vortices have split are not symmetric with respect to the symmetry plane. Instead they appear to be alternating in position relative to the symmetry plane. A schematic representation of such a pattern of alternating counter-rotating pairs is given in figure 20.

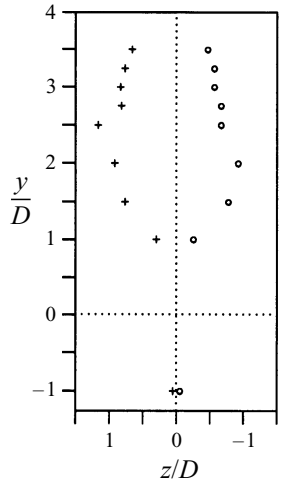

FIGURE 21. z/D locations of centres of $\langle\omega_y\rangle$-circulations deduced from horizontal plane results at $x/D = 7$ with $s_c = 4.8$ (e.g. figures 16(*a*)–16(*c*)). +, counter-clockwise structures; ○, clockwise structures.

Figure 21 displays the z/D locations of the centres of $\langle\omega_y\rangle$-circulation as obtained in the horizontal planes with $s_c = 4.8$. Unlike the equivalent results obtained with $s_c = 1.6$ (figure 10), these vortex spacings are not symmetric for $y/D > 2$. This lack of symmetry throughout the top region the jet-wake ($y/D > 2$) is indicative of an asymmetrically alternating counter-rotating vortex pattern as identified in figure 16(*c*) for $y/D = 2.75$.

10. Fine-scale turbulence levels

In this section the ensemble-averaged fine-scale turbulence levels ($\langle$FSTIF$\rangle$) in the stack-wake, the jet-wake and the bent-over jet will be discussed. These results will serve to support the earlier conclusions made and will also allow us to identify the entrainment processes associated with the jet-wake structures. The $\langle$FSTIF$\rangle$ levels are obtained from the instantaneously computed values of the fine-scale turbulence indicator function (Ferré *et al.* 1990). The levels are plotted for the 10, 20, …, 90 and 95% levels of a specified peak value (0% is the free-stream value).

10.1. *Horizontal planes*

The previously shown $\langle u_c\rangle/U_{cf}\,\hat{\boldsymbol{i}} + \langle w_c\rangle/U_{cf}\,\hat{\boldsymbol{k}}$ velocity-vector patterns and streamlines which were obtained in the horizontal planes with $s_c = 4.8$ are now displayed in superposition with $\langle$FSTIF$\rangle$. These superpositions are shown in figures 22(*a*)–(*d*) for $y/D = -1$, 1, 2.75 and 3.75, respectively. The $\langle$FSTIF$\rangle$ scale is identical for all these positions, such that comparisons can be made, and is based on the highest peak value, which is at $y/D = 3.75$.

The $\langle$FSTIF$\rangle$ pattern in figure 22(*a*) at $y/D = -1$ bears a close resemblance to the intermittency function iso-contours levels in figure 22 of Cantwell & Coles (1983), as expected. It is evident that high-turbulence activity (dark greys or high $\langle$FSTIF$\rangle$ is associated with the structures, with the maximum turbulent activity lying slightly above the centre of the structures. Furthermore, a wavy boundary separating the outer 'potential' fluid (white or low $\langle$FSTIF$\rangle$) and the turbulent wake can be observed. The

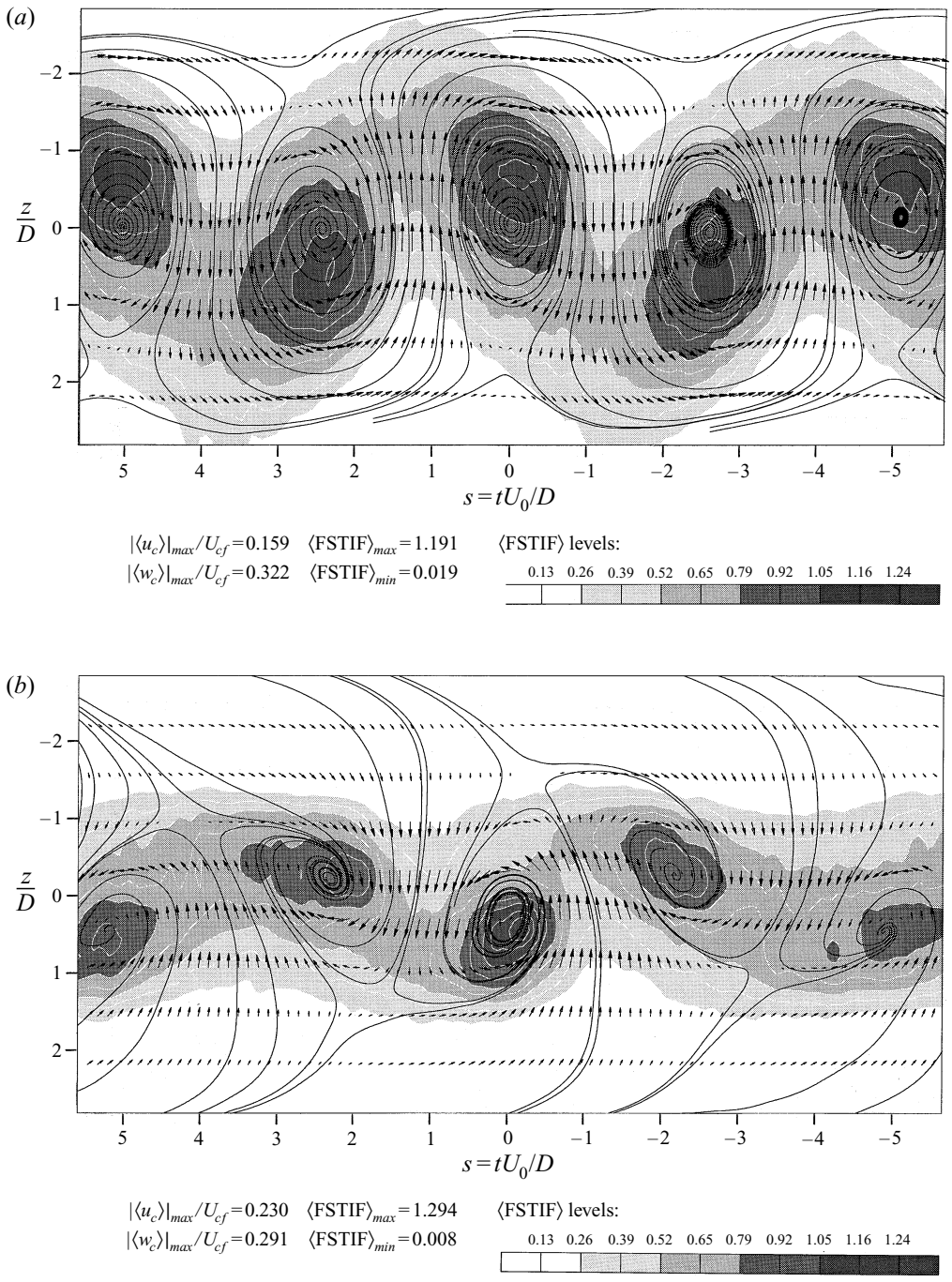

FIGURE 22(*a*, *b*). For caption see facing page.

indentations of 'potential' fluid on the upstream side of the structures suggest that 'potential' fluid is being entrained between two adjacent structures. However, it can also be seen that there is a wide 'band' of streamlines that wind around the alternating structures (similar to the results by Zhou & Antonia 1993). According to this 'band'

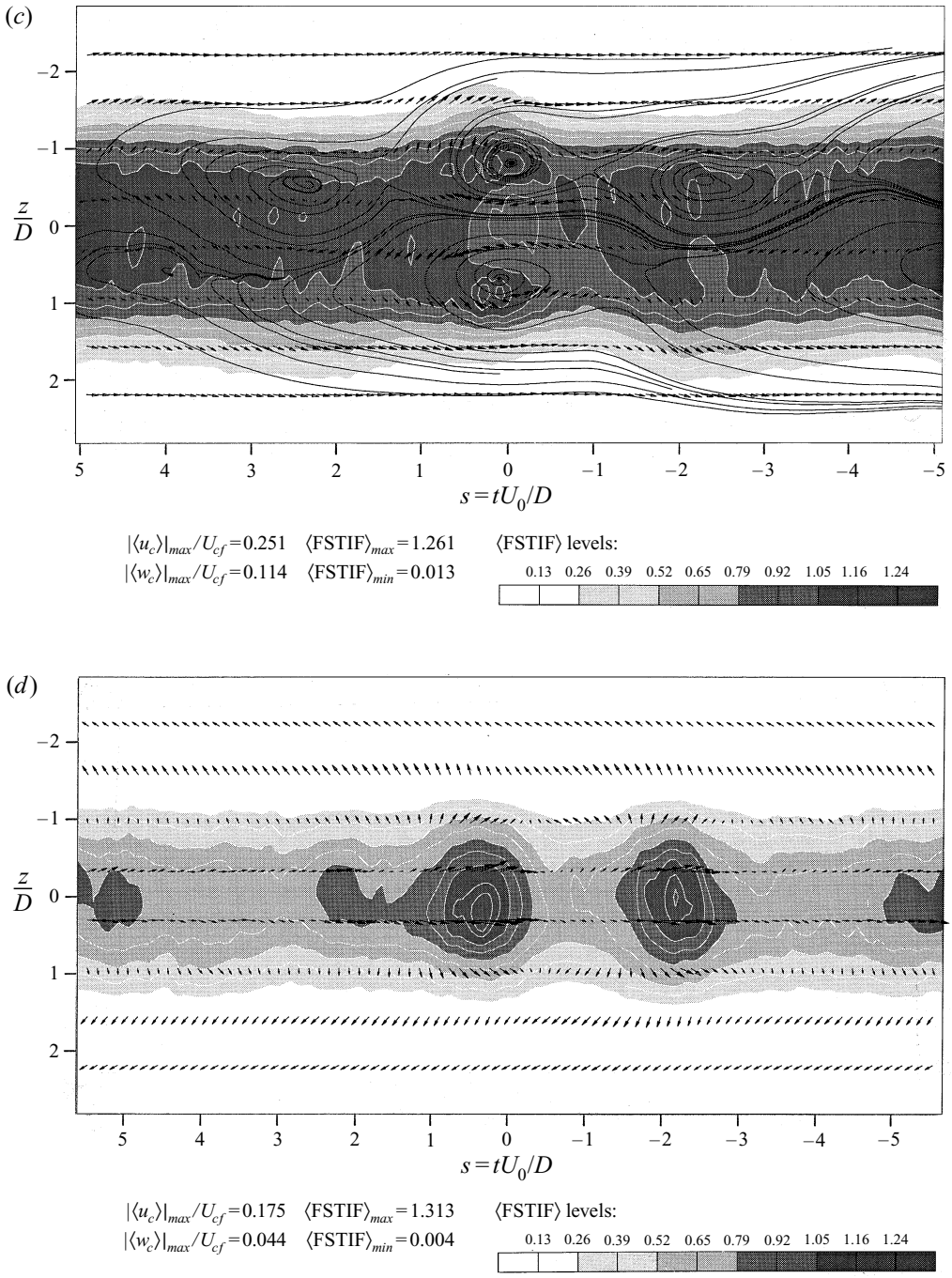

FIGURE 22. $\langle u_c\rangle/U_{cf}\,\hat{\boldsymbol{i}}+\langle w_c\rangle/U_{cf}\,\hat{\boldsymbol{k}}$ velocity vectors, sectional streamlines and $\langle$FSTIF$\rangle$ fine-scale turbulence iso-contours in four horizontal planes at $x/D = 7$. (*a*) $y/D = -1$; (*b*) $y/D = 1$; (*c*) $y/D = 2.75$; (*d*) $y/D = 3.75$. $s_c = 4.8$. Note, no sectional streamlines are given for (*d*).

there does not appear to be much fluid actually entrained by the structures. However, it should be remembered that the results presented herein, as well as those of Zhou & Antonia (1993), are actually evolutions in time at constant y/D rather than evolutions in space. Thus, the downstream growth of the structures owing to entrainment cannot be represented by these results. The results of Cantwell & Coles (1983), on the other hand, though they are based on streamwise measurements, cannot account for the acceleration (change in U_{cv}) of the structures.

In figure 22(*b*), at $y/D = 1$, the jet-wake vortices can be readily identified with the $\langle$FSTIF$\rangle$ iso-contours. The area circumscribed by the 0.79 iso-contour level of the central structures is smaller at $y/D = 1$ than at $y/D = -1$, and the peak value is slightly higher at $y/D = 1$. This is consistent with the peak vorticity results, which suggest that the jet-wake vortices are being stretched near $y/D = 1$. It should also be observed that the width of the wake, arbitrarily defined by the 0.26 $\langle$FSTIF$\rangle$ level is narrower than at $y/D = -1$, and is in fact narrower than at any other lateral location in the jet-wake.

The indentations of 'potential' fluid at $y/D = 1$ (figure 22*b*) are not as deep as they are at $y/D = -1$ (figure 22*a*). However, in contrast to $y/D = -1$, there is now a significant amount of 'potential' fluid that enters the region between alternating vortices. This significant inflow of potential fluid is perhaps the reason for the flow visualizations of Fric & Roshko (1994) which show 'nearly closed' streaklines in the jet-wake, as opposed to 'separating streaklines' in the case of shedding behind a cylinder. With regard to the issue of whether the jet sheds some of its vorticity, these results suggest that owing to the large amount of entrainment, the cores of the jet-wake vortices, which we maintain are essentially jet-fluid vortices, will be significantly diluted by the influx of 'potential' crossflow fluid. This is consistent with the observations of relatively weak fingers of jet-fluid observed by Lozano *et al.* (1994).

Figure 22(*c*), at $y/D = 2.75$, shows strong turbulent activity associated with the counter-rotating pair of split jet-wake vortices, thereby supporting the existence of these structures. Interestingly, there appears to be fluid at lower turbulence levels trapped on the downstream side of the centre of the counter-rotating vortex structures. The higher turbulent activity is concentrated on the upstream side of the structures. Also, the fine-scale activity bulges out toward the freestream on the upstream side of both vortices located near $s = 0$. Furthermore, apart from the concentrations of $\langle$FSTIF$\rangle$ associated with the structures near $s = 0$, no adjacent structures can be identified via $\langle$FSTIF$\rangle$, since $\langle$FSTIF$\rangle$ appears high throughout the core of the wake. Finally, no periodicity associated with $\langle$FSTIF$\rangle$ can be distinguished anymore, apparently owing to smearing, although the periodicity is still extracted from the large-scale activity. These observations will be compared to the vertical plane results in §10.2.

Figure 22(*d*), at $y/D = 3.75$, coinciding with the centreline of the bent-over jet, reveals periodically occurring regions of strong turbulent activity congruent with the concentrations of strong streamwise velocities identified earlier with the tops of the bridges (refer to figure 19 and §9.4). The spacing between the two strongest regions of $\langle$FSTIF$\rangle$ reveals that St_D is about 0.38, in agreement with the nominal frequency expected from the cross-linked configuration. Although this is the location of the core of the jet, the $\langle$FSTIF$\rangle$ contours defining the structures are now better isolated than in the wake region below at $y/D = 2.75$. At first thought this is surprising, but, on careful reflection, it is seen to be in agreement with the strong streamwise inclination of the jet-wake vortices which will tend to cause high levels of turbulent activity to be detected along extended streamwise portions near $y/D = 2.75$. Above the bridging point at $y/D = 3.75$, however, only the 'tops' of these structures are detected. It should

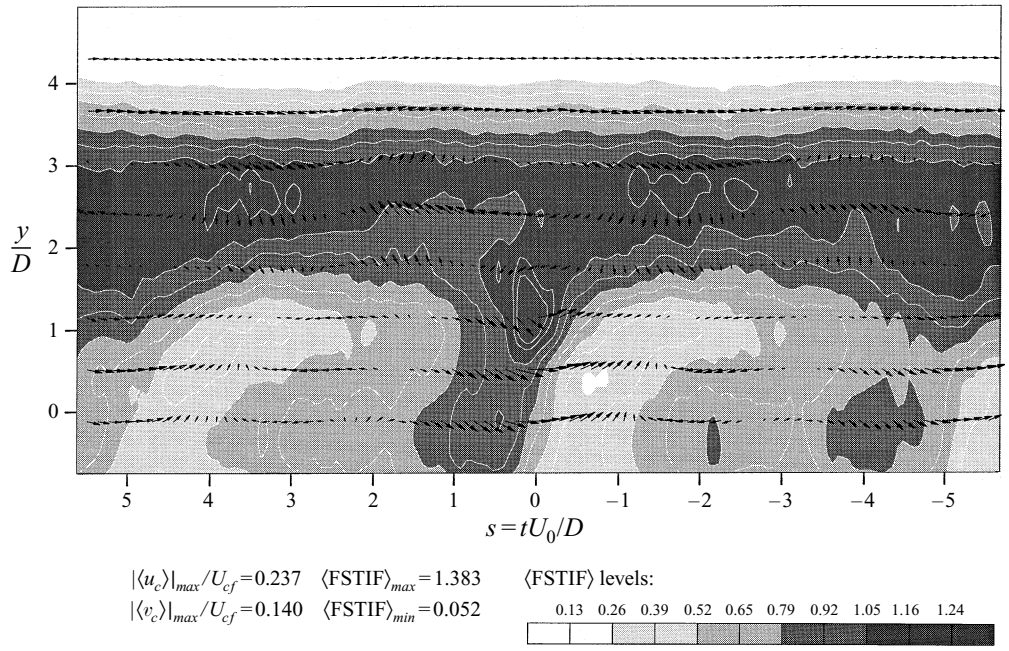

FIGURE 23. $\langle u_c\rangle/U_{cf}\,\hat{\boldsymbol{i}}+\langle v_c\rangle/U_{cf}\,\hat{\boldsymbol{j}}$ velocity vectors and $\langle$FSTIF$\rangle$ fine-scale turbulence iso-contours in vertical plane at $x/D = 7$, $z/D = -0.5$. $s_c = 1.6$.

be stressed that this implies that the jet-wake vortices have penetrated the core of the jet. Furthermore, the highest levels of turbulent activity in the core of the jet are evidently connected to events controlled by the stack.

10.2. *Vertical planes*

Figure 23 shows $\langle$FSTIF$\rangle$ superimposed upon the $\langle u_c\rangle/U_{cf}\,\hat{\boldsymbol{i}}+\langle v_c\rangle/U_{cf}\,\hat{\boldsymbol{j}}$ velocity-vector pattern shown earlier in figure 12. The results are in the $z/D = -0.5$ vertical plane. Again the $\langle$FSTIF$\rangle$ levels are based on the peak value in the horizontal plane at $y/D = 3.75$. In the lower region of the wake, the lateral extent of the jet-wake vortices can be clearly identified by the 'legs' of high $\langle$FSTIF$\rangle$. The lower levels of $\langle$FSTIF$\rangle$ are evidence of the penetration of 'potential' fluid between adjacent structures.

The results presented in the horizontal planes are consistent with those in this vertical plane. For example, in the upper portion of the wake, near $y/D = 2.75$, $\langle$FSTIF$\rangle$ appears almost constant for all s in figure 23. These uniform $\langle$FSTIF$\rangle$ levels, which are in the $z/D = -0.5$ plane, are consistent with the basically uniform level of $\langle$FSTIF$\rangle$ for all s at $z/D = -0.5$ in figure 22(c), which is at $y/D = 2.75$. In other words, the $\langle$FSTIF$\rangle$ levels at the line where the two orthogonal planes displayed in figure 23 and figure 22(c) intersect, are in agreement. Furthermore, the slight increase of $\langle$FSTIF$\rangle$ on the upstream side of structures near $s \sim 0.5$ to -0.25 in figure 22(c) is also consistent with the slight increases of $\langle$FSTIF$\rangle$ near $s \sim -1$ to -2.5 at $y/D = 2.75$ in figure 23, if the structures are inclined in the positive streamwise direction as shown in §9.5. This provides further evidence that the structures are inclined in the downstream direction.

Figure 24 shows $\langle$FSTIF$\rangle$ superimposed upon the $\langle u_c\rangle/U_{cf}\,\hat{\boldsymbol{i}}+\langle v_c\rangle/U_{cf}\,\hat{\boldsymbol{j}}$ vectors and sectional streamlines with regard to the vertical plane vectors at $z = 0$ already

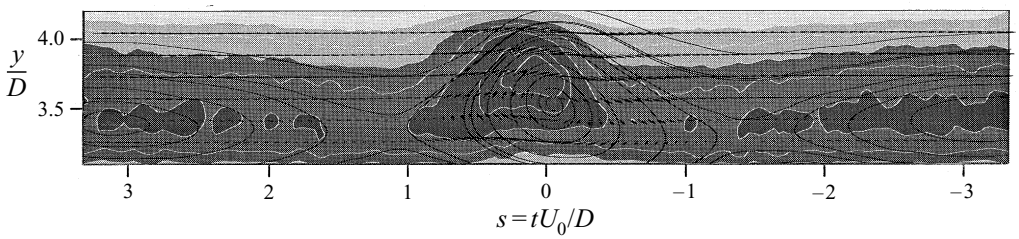

FIGURE 24. $\langle u_c\rangle/U_{cf}\,\hat{\boldsymbol{i}}+\langle v_c\rangle/U_{cf}\,\hat{\boldsymbol{j}}$ velocity vectors, sectional streamlines, $\langle$FSTIF$\rangle$ fine-scale turbulence iso-contours in vertical plane at $x/D = 7$, $z/D = 0$. $s_c = 1.6$.

displayed in figure 17. The $\langle$FSTIF$\rangle$ levels are based on the local peak value. The results reveal a vertical 'cross-section' of the bridges. It can be seen that $\langle$FSTIF$\rangle$ is higher on the back of the structures, with highly turbulent fluid almost being ejected to the crossflow on top of the jet. The strong region of turbulent activity penetrates the bent-over jet region and in fact peaks on the jet-centreline. This is where the highest value of $\langle$FSTIF$\rangle$ has been found in any of the horizontal or vertical planes investigated at this x/D location.

The penetration of more potential fluid on the downstream side of the structures helps to clarify the earlier identification of fluid at lower turbulence levels trapped in between two counter-rotating structures in the horizontal plane (figure 22(*c*), $y/D = 2.75$). Freestream fluid appears to be engulfed on the downstream side and near the centre of the bridges and then proceeds to become turbulent as it passes between the 'legs' of the jet-wake vortices.

11. Concluding remarks

It was previously shown by Eiff *et al.* (1995), that the Kármán-like vortex structures in the stack-wake are locked to Kármán-like vortex structures in the jet-wake and are both characterized by the Strouhal frequency based on the stack diameter. In this paper, we have established that the Kármán-like vortex structures in the jet-wake, which we refer to as jet-wake vortices, extend to just below the centreline of the jet on each side of the symmetry plane of the flow. Furthermore, a cross-link configuration describing the connections of the vortices was found to be consistent with the results in all the planes investigated. The two central aspects of the cross-link configuration are that the vortices split in the jet-wake and that they are linked to each other just below the centreline of the jet.

The pattern-recognition technique is able to detect and align single structures with non-periodic occurrences, but in order to obtain a clear ensemble-average of two or more structures within a repetitive structural pattern, a relatively sharp probability distribution of the occurrence (i.e. arrival times) of the structures is required. The lock-in between the vortices in the stack-wake and the vortices in the jet-wake provided a level of quasi-periodicity which allowed the direct verification of the frequency aspect of the cross-link configuration – even in the core of the jet. We would expect the jet-wake vortices in ground-level jets to be split as well, where an interaction between horse-shoe vortices at the foot of the jet and the jet-wake vortices exists (Fric & Roshko 1994). However, the horse-shoe vortices are likely to be less periodic, leading to a

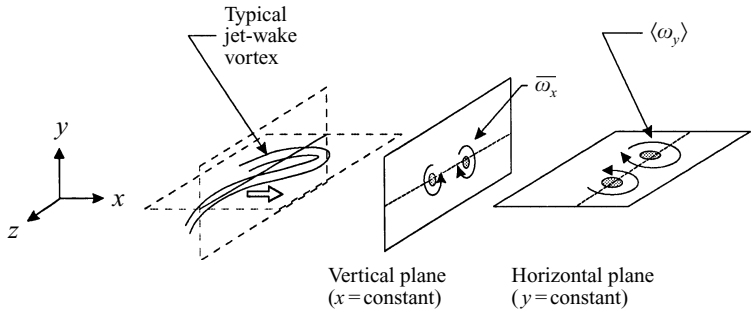

FIGURE 25. View of two orthogonal planes intersecting a typical jet-wake vortex convecting past the planes. Mean measurements in a vertical plane reveal a mean counter-rotating vortex pair with $\overline{\omega_x}$ (e.g. Andreopoulus & Rodi 1984). PRT results in a horizontal plane below the centreline of the bent-over jet revealing a pair of time-dependent counter-rotating vortices with $\langle\omega_y\rangle$ (e.g. figure 16*c*).

broader PDF of occurrence of the vortices behind the jet. This would make the frequency aspect of the cross-link configuration more difficult to verify.

One feature in this flow which has been investigated is the well-known mean counter-rotating vortex pair, because it is reflected in a mean flow pattern in (x = constant)-planes, which can be readily measured or predicted by steady-state turbulence models (Ni *et al.* 1993). However, what is the underlying time-dependent motion associated with this mean field? Even the unsteady simulation by Rudman (1996) of a jet issuing from a ground-level source at very low Reynolds numbers has not provided a clear answer to this question.

The present results have shown time-dependent structures in (y = constant)-planes, but could these structures account for the observed mean motion in (x = constant)-planes? The streamwise inclined vortex lines of the split jet-wake vortices form a pair of time-dependent counter-rotating vortices with vorticity components ω_x and ω_y. We have been able to extract realizations containing such time-dependent vortices, yielding ensemble-averaged $\langle\omega_y\rangle$ contours. However, the ω_x-component of the inclined time-dependent counter-rotating vortices is consistent with the vorticity of the mean counter-rotating vortex pair usually measured in (x = constant)-planes, as suggested in the exploded view of the jet-wake vortices in the two orthogonal planes in figure 25. It is thus likely that vorticity due to the Kármán-like jet-wake vortices contributes to the mean vorticity of the counter-rotating vortex motion. Such a relationship is also suggested by a comparison of the alternating pattern of the ensemble-averaged counter-rotating vortex pattern depicted in figure 20 and the results of Smith *et al.* (1993). Smith *et al.* determined that the concentration of the counter-rotating vortex pair (in (x = constant)-planes) was instantaneously asymmetrical and appeared to alternate with respect to the symmetry plane.

Measurements at stations closer to the exit of the jet are more difficult to undertake owing to the existence of a recirculating zone, high turbulence intensities and the angle of the mean flow. However, preliminary results at $x/D = 3$ have indicated that the cross-link configuration is already present at least at this stage in the flow. This fact plus the relationship between the mean counter-rotating vortex pair and the ensemble-averaged time-dependent counter-rotating pair resulting from the split Kármán-like jet-wake vortices suggest that the origin of both motions is near the jet exit, where the jet-wake vortices are being shed. We speculate that the stack-wake vortices control the formation of the jet-wake vortices whose top portion remain attached to the jet. As the jet-wake structures proceed to be convected downstream, the lower, shed, portion is

being stretched along its axis and also into the downstream direction because the jet moves faster than the crossflow fluid for $R > 1$. This stretching into the downstream direction accounts for the observed counter-rotating vortex motion.

It should be stressed that the jet-wake structures contain jet fluid; their vorticity originates in the jet's shear layer. The details of how the jet-wake vortices are attached to the jet have been shown in this paper. In order to satisfy the solenoidal condition they must remain connected. As demonstrated, this connection is provided by the bridge of the cross-link configuration. Another requirement is that the vortices must split. These splitting points, or nodes, have been shown to exist for the 'two-dimensional' equivalent flow, i.e. the plane wake (Taneda 1952). In the plane wake, however, these nodes are usually buried within the boundary layers at the ends of the 'two-dimensional' flow.

What happens for changing flow parameters? The most significant is the velocity ratio as it affects the mean statistics of the flow markedly. Eiff & Keffer (1995) and Eiff (1996) examined whether or not the lock-in between the stack-wake vortices and the jet-wake vortices is present for a range of velocity ratios as well as jet-to-stack diameter ratios. For the velocity ratios considered, $R = 1.5$, 3 and 6, it was found that the lock-in exists down to values of the diameter ratio of about 0.5.

This research was supported by the Natural Sciences and Engineering Research Council of Canada through Grant A-2746 and NATO through Grant CRG-960142. We would like to thank J. Ferré and F. Giralt for the use of their pattern-recognition codes.

REFERENCES

Andreopoulos, J. & Rodi, W. 1984 Experimental investigation of jets in crossflow. *J. Fluid Mech.* **138**, 93–127.

Cantwell, B. & Coles, D. 1983 An experimental study of entrainment and transport in the turbulent near wake of a circular cylinder. *J. Fluid Mech.* **136**, 321–374.

Crabb, D., Durão, D. F. G. & Whitelaw, J. H. 1981 A round jet normal to a crossflow. *J. Fluids Engng* **103**, 142–153.

Eiff, O. S. 1996 Experimental analysis of the coherent structures within a turbulent jet in a crossflow. PhD thesis, University of Toronto.

Eiff, O. S., Kawall, J. G. & Keffer, J. F. 1995 Lock-in of vortices in the wake of an elevated round turbulent jet in a crossflow. *Exps. Fluids* **19**, 203–213.

Eiff, O. S. & Keffer, J. F. 1995 Limits of the lock-in mechanism in a round turbulent jet emitted from an elevated source. *15th Canadian Congr. Appl. Mech.* University of Victoria, Victoria, British Columbia.

Fearn, R. & Weston, R. P. 1974 Vorticity associated with a jet in a cross flow. *AIAA J.* **12**, 1666–1671.

Ferré, J. A. & Giralt, F. 1989 Pattern-recognition analysis of the velocity field in plane turbulent wakes. *J. Fluid Mech.* **198**, 27–64.

Ferré, J. A., Mumford, J. C., Savill, A. M. & Giralt, F. 1990 Three-dimensional large-eddy motions and fine-scale activity in a plane turbulent wake. *J. Fluid Mech.* **210**, 371–414.

Fric, T. F. & Roshko, A. 1994 Vortical structure in the wake of a transverse jet. *J. Fluid Mech.* **279**, 1–47.

Huang, R. F. & Chang, J. M. 1994 Coherent structure in a combusting jet. *AIAA J.* **32**, 1120–1125.

Hussain, A. K. M. F. 1983 Coherent structures-reality or myth. *Phys. Fluids* **20**, 2816–2849.

Hussain, A. K. M. F. & Hayakawa, M. 1987 Eduction of large-scale organized structures in a plane turbulent wake. *J. Fluid Mech.* **180**, 193–229.

Kamatoni, Y. & Greber, I. 1972 Experiments on a turbulent jet in a cross flow. *AIAA J.* **10**, 1425–1429.

KEFFER, J. F. & BAINES, W. D. 1963 The round turbulent jet in a cross-wind. *J. Fluid Mech.* **15**, 481–496.

KELSO, R. M., LIM, T. T. & PERRY, A. E. 1996 An experimental study of round jets in cross-flow, *J. Fluid Mech.* **306**, 111–144.

KOPP, G. A., KAWALL, J. G. & KEFFER, J. F. 1995 The evolution of the coherent structures in a uniformly distorted plane turbulent wake. *J. Fluid Mech.* **291**, 299–322.

LOZANO, A., SMITH, S. H., MUNGAL, M. G. & HANSON, R. K. 1994 Concentration measurements in a transverse jet by planar laser-induced fluorescence of acetone. *AIAA J.* **32**, 218–221.

MCMAHON, H. M., HESTER, D. D. & PALFREY, J. G. 1971 Vortex shedding from a turbulent jet in a cross-wind. *J. Fluid Mech.* **48**, 73–80.

MORTON, B. R. & IBBETSON, A. 1996 Jets deflected in a crossflow. *Expl Thermal Fluid Sci.* **12**, 112–133.

MOUSSA, Z. M., TRISCHKA, J. W. & ESKINAZI, S. 1977 The near field in the mixing of a round jet with a cross-stream. *J. Fluid Mech.* **80**, 49–90.

MUMFORD, J. C. 1982 The structure of large eddies in fully developed turbulent shear flows. Part 1. The plane jet. *J. Fluid Mech.* **118**, 241–268.

NI, W., KAWALL, J. G. & KEFFER, J. F. 1993 On the velocity and temperature fields of a heated turbulent jet in cross-flow. *Inaugural Conf. CFD Soc. Canada, Montréal*, pp. 339–350.

PERRY, A. E. & CHONG, M. S. 1987 A description of eddying motions and flow patterns using critical-point concepts. *Ann Rev. Fluid Mech.* **19**, 125–153.

RUDMAN, M. 1996 Simulation of the near field of a jet in a cross flow. *Expl Thermal Fluid Sci.* **12**, 134–141.

SMITH, S. H., LOZANO, A., MUNGAL, M. G. & HANSON, R. K. 1993 Scalar mixing in the subsonic jet in crossflow. *AGARD Jet in Cross Flow Symp.*, pp. 6.1–6.13. Winchester, UK.

SYKES, R. I., LEWELLEN, W. S. & PARKER, S. F. 1986 On the vorticity dynamics of a turbulent jet in a crossflow. *J. Fluid Mech.* **168**, 393–413.

TANEDA, S. 1952 Studies on wake vortices (I). *Rep. Res. Inst. Appl. Mech.* **1**(4), 131.

ZHOU, Z. & ANTONIA, R. A. 1993 A study of vortices in the near wake of a cylinder. *J. Fluid Mech.* **253**, 643–661.